Redox Biology 59 (2023) 102585

Contents lists available at ScienceDirect

Redox Biology

journal homepage: www.elsevier.com/locate/redox

Hindering NAT8L expression in hepatocellular carcinoma increases cytosolic aspartate delivery that fosters pentose phosphate pathway and purine biosynthesis promoting cell proliferation

Pamela De Falco [a], Giacomo Lazzarino [b], Federica Felice [a], Enrico Desideri [c], Serena Castelli [d], Illari Salvatori [e,f], Fabio Ciccarone [a,d,**,1], Maria Rosa Ciriolo [a,d,*,1]

[a] Department of Biology, University of Rome "Tor Vergata", Via Della Ricerca Scientifica, 00133, Rome, Italy
[b] UniCamillus-Saint Camillus International University of Health and Medical Sciences, Via di Sant'Alessandro 8, 00131, Rome, Italy
[c] IRCCS San Raffaele Roma, Department of Human Sciences and Promotion of the Quality of Life, San Raffaele Roma Open University, Via di Val Cannuta, 247, 00166, Rome, Italy
[d] IRCCS San Raffaele Roma, Via di Val Cannuta, 247, 00166, Rome, Italy
[e] IRCCS Fondazione Santa Lucia, Via Del Fosso di Fiorano 64, Rome, 00143, Italy
[f] Department of Experimental Medicine, Sapienza University of Rome, 00161, Rome, Italy

ARTICLE INFO

Keywords:
NAA
Aspartate
Nucleotides
Pentose phosphate pathway
Mitochondria

ABSTRACT

N-acetylaspartate (NAA) is synthesized by the mitochondrial enzyme NAT8L, which uses acetyl-CoA and aspartate as substrates. These metabolites are fundamental for bioenergetics and anabolic requirements of highly proliferating cells, thus, NAT8L modulation may impinge on the metabolic reprogramming of cancer cells. Specifically, aspartate represents a limiting amino acid for nucleotide synthesis in cancer.

Here, the expression of the NAT8L enzyme was modulated to verify how it impacts the metabolic adaptations and proliferative capacity of hepatocellular carcinoma. We demonstrated that NAT8L downregulation is associated with increased proliferation of hepatocellular carcinoma cells and immortalized hepatocytes. The overexpression of NAT8L instead decreased cell growth. The pro-tumoral effect of NAT8L silencing depended on glutamine oxidation and the rewiring of glucose metabolism. Mechanistically, NAT8L downregulation triggers aspartate outflow from mitochondria via the exporter SLC25A13 to promote glucose flux into the pentose phosphate pathway, boosting purine biosynthesis. These results were corroborated by the analyses of human and mouse hepatocellular carcinoma samples revealing a decrease in NAT8L expression compared to adjacent non-tumoral tissues. Overall, this work demonstrates that NAT8L expression in liver cells limits the cytosolic availability of aspartate necessary for enhancing the pentose phosphate pathway and purine biosynthesis, counteracting cell proliferation.

1. Introduction

Hepatocellular carcinoma (HCC) accounts for ~90% of liver cancer cases [1], and it is the fourth most common cause of cancer-related deaths worldwide [2]. HCC onset is linked to differential risk factors such as virus infections (HCV and HBV), cirrhosis and non-alcoholic steatohepatitis (NASH) [1]. HCC treatments are strictly related to the patients' cancer stage: ablation, resection and liver transplantation occur in the early-stage HCC; locoregional treatments occur in the intermediate stages; targeted receptor tyrosine kinase inhibitors or immunotherapy are considered in the advanced stage [3]. Identifying new determinants of HCC development and progression, including cancer-specific metabolic traits, may provide new therapeutic hints to overcome the increasing problem of chemoresistance to the drugs currently in use [4].

Cancer cells rewire their metabolism to provide energy and neosynthetized macromolecules necessary for increasing the proliferation rate. The metabolic reprogramming is mainly drawn by microenvironment limitations and the effect of oncogenic pathways on the tissue-of-

* Corresponding author. Department of Biology, University of Rome "Tor Vergata", Via Della Ricerca Scientifica, 00133, Rome, Italy.
** Corresponding author. Department of Biology, University of Rome "Tor Vergata", Via Della Ricerca Scientifica, 00133, Rome, Italy.
E-mail addresses: fabio.ciccarone@uniroma2.it (F. Ciccarone), ciriolo@bio.uniroma2.it (M.R. Ciriolo).
[1] F.C. and M.R.C. equally contributed as co-last authors.

https://doi.org/10.1016/j.redox.2022.102585
Received 18 October 2022; Received in revised form 5 December 2022; Accepted 21 December 2022
Available online 24 December 2022

Abbreviations

HCC	Hepatocellular carcinoma
NAA	N-acetylaspartate
NAT8L	N-acetyltransferase 8-like
ASPA	Aspartoacylase
NASH	Non-alcoholic steatohepatitis
SCR	Scramble
2-DG	2-deoxyglucose
PDH	Pyruvate dehydrogenase
BPTES	Bis-2-(5-phenylacetamido-1,3,4-thiadiazol-2-yl)ethyl sulfide
GLUT1	Glucose transporter 1
HK-2	Hexokinase-2
PKM2	Pyruvate kinase isozyme M2
UDP-GlcNac	UDP-N-acetylglucosamine
PPP	Pentose phosphate pathway
G6PD	Glucose-6-phosphate dehydrogenase
6-AN	6-aminonicotinamide
MTR	MitoTracker Red
MTG	MitoTracker Green
GSSG	Glutathione disulfide
GSH	Glutathione
UMP	Uridine monophosphate
IMP	Inosine monophosphate
HPRT1	Hypoxanthine Phosphoribosyltransferase 1
PPAT	Phosphoribosyl Pyrophosphate Amidotransferase
GART	Phosphoribosylglycinamide Formyltransferase
ADSL	Adenylosuccinate Lyase
PFAS	Phosphoribosylformylglycinamidine Synthase
ATIC	5-Aminoimidazole-4-Carboxamide Ribonucleotide Formyltransferase/IMP Cyclohydrolase
PRPP	Phosphoribosyl pyrophosphate
SLC	Solute carrier
6-MP	6-mercaptopurine
T	Tumoral
NT	Non tumoral
CDD	Choline deficient diet
DEN	Diethylnitrosamine
BrdU	Bromodeoxyuridine
TFAM	Transcription Factor A Mitochondrial
ATGL	Adipose triglyceride lipase
MFI	Mean fluorescence intensity
ECAR	Extracellular acidification rate
OCR	Oxygen consumption rate
SRC	Spare respiratory capacity
TCGA-LIHC	The Cancer Genome Atlas Liver Hepatocellular Carcinoma
GSE	Gene Set Enrichment

origin, even though cancer cells activate common metabolic pathways to satisfy their proliferative and survival requirements [5,6]. The rearrangement of glucose metabolism is fundamental for the maintenance of cancer cells in terms of energy and anabolic outputs. Beyond providing ATP rapidly by the aerobic glycolytic system known as "the Warburg effect", glucose is massively channeled into the pentose phosphate pathway (PPP) for generating NADPH, which is necessary for redox homeostasis, antioxidant defense and the production of ribose-5-phosphate used in the nucleotide biosynthesis [7]. Nowadays, the biosynthetic contribution of mitochondria is also well-recognized in cancer cells, which consume different fuels, particularly glutamine, for feeding cataplerotic reactions of the Krebs' cycle [8,9]. Mitochondrial metabolism oxidizes acetyl-CoA or glutamine-derived 2-oxoglutarate for bioenergetic purposes, but it also contributes to cell growth by providing aspartate, which is limiting for nucleotide biosynthesis and thus proliferation [10,11]. The importance of aspartate in sustaining proliferation is further evidenced by the fact that tumor cells can increase the amount of aspartate by over-expression of the plasma membrane aspartate importer Solute carrier (SLC) family 1 member A3 (SLC1A3) [12,13] thus overcoming disadvantageous conditions such as mitochondrial impairment or glutamine restriction [14,15].

The mitochondrial enzyme SHATI/N-acetyltransferase 8-like (hereafter referred to as NAT8L) synthetizes N-acetylaspartate (NAA) starting from acetyl-CoA and aspartate. Once produced, NAA can be catabolized in the cytosol by the aspartoacylase (ASPA) enzyme, which produces acetate and aspartate. NAA is mainly known for its role in the central nervous system, where acetate-derived acetyl-CoA is employed in synthetizing myelin and where an alteration in NAA levels is correlated with neurodegenerative disorders [16]. Recently, a role for NAA has also been discovered in peripheral tissues. For instance, NAA synthesis is increased during the browning process of adipose tissue and in some tumor types, such as ovarian and non-small lung cancer [17–20].

Our recent work demonstrated that boosting mitochondrial oxidative metabolism by sustained lipid catabolism was effective in reducing the proliferation of HCC cells [21]. Considering that NAA synthesis may impact the availability of mitochondrial acetyl-CoA and aspartate, we evaluated whether the modulation of NAT8L expression influences the proliferation and metabolism of the HCC cell line HepG2 and the immortalized hepatocytes HuS-E/2. Our data indicated that NAT8L silencing promotes cell growth by inducing an extensive rewiring of mitochondrial and glucose metabolism that ultimately results in increased PPP activation and cytosolic aspartate availability necessary for purine biosynthesis. These results are corroborated by the down-regulation of NAT8L protein in HCC tumor biopsies.

2. Materials and methods

2.1. Cell culture

HepG2 and HuH7 cells, from European Collection of Cell Culture (ECACC), were grown respectively in RPMI and in DMEM supplemented with 10% fetal bovine serum, 10 U/ml penicillin/streptomycin and 2 mM L-glutamine. HuS-E/2 cells were kindly provided by Dr. Vinicio Carloni (University of Florence) and were grown in DMEM containing 4.5 g/L of glucose supplemented with 10% FBS, 5 ng/ml EGF (Sigma-Aldrich, E9644), 0.42 μg/ml insulin (Sigma-Aldrich, I9278), 20 ng/ml selenium (Sigma-Aldrich, S9133), 1% DMSO (AMRESCO®, 0231), 10 U/ml penicillin/streptomycin and 2 mM L-glutamine. Cells were periodically tested for mycoplasma according to protocols from our laboratory. Cells were cultured at 37 °C in an atmosphere of 5% CO_2 in air.

2.2. Materials

Cell culture medium and supplements are from EuroClone S.p.A. Triton™ X-100 (T9284), Sodium Deoxycholate (D6750), Sodium Fluoride (S7920), Sodium pyrophosphate (221,368), Sodium orthovanadate (S6508), 2-β-mercaptoetanol (M6250), blue of bromophenol (B5525), NAD^+ (N7004), LDH (10,127,230,001), NP-40 (74,385), ATP (A26209), $NADP^+$ (N0505), Glucose-6-phosphate dehydrogenase (G7877), Glucose-6-phosphate (G7879), 6-phosphogluconate (P7877), 2-deoxyglucose (2-DG) (D6134), 6-aminonicotinamide (6-AN) (A68203), Bis-2-(5-phenylacetamido-1,3,4-thiadiazol-2-yl)ethyl sulfide (BPTES) (SML0601), 6-mercaptopurine (6-MP) (852,678), oligomycin and

formalin solution neutral buffered 10% (4% paraformaldehyde containing) (HT5012) are from Sigma-Aldrich. Sodium pyruvate is from Gibco.

2.3. Transfections

The following siRNA sequences were used to transfect cells: NAT8L-KD1 (Sigma Aldrich, 5′-GCAUGACUUUAAUUCUUGGGA-3′); NAT8L-KD2 (Sigma Aldrich, 5′-CGGACAUCGAGCAGUACUACA-3′); ADSL (Sigma Aldrich, 5′-UAUUCAAUAUAGUAUCUGCGG-3′); PPAT (Sigma Aldrich, 5′-UUUGCACCAGAUUCUUUGAGC-3′), G6PD (Santa Cruz Biotechnology, sc-60667), AGC2 (Life Technologies, s532443); MISSION® siRNA Universal Negative Control #1 (SIC001) was used as scrambled siRNA control. All siRNA were transfected using Lipofectamine® 3000 (Invitrogen), according to the manufacturer's instruction and used at the final concentration 10 nM. To overexpress NAT8L enzyme we used plasmid pDEST26/NAT8L and as negative control plasmid pDEST26 through the jetOPTIMUS according to the manufacturer's instructions.

2.4. Western blot analysis

Cells pellets were resuspended in a lysis buffer (50 mM Tris-HCl, pH 7.4, 150 mM NaCl, 1 mM EDTA, 1% Triton™ X-100, 0.5% Sodium Deoxycholate, 0.1% SDS, 10 mM sodium fluoride, 5 mM Sodium Pyrophosphate, 2 mM Sodium Orthovanadate) supplemented with protease inhibitor cocktail (Sigma-Aldrich, PIC0002). For NAT8L determination, analysis was performed on supernatants obtained after lysis of cell pellets in nuclei extraction buffer (10 mM Tris-HCL, 10 mM $MgCl_2$, 1 mM EDTA, 0.25 M sucrose, 1% Triton™ X-100, 50 mM sodium fluoride, 2 mM Sodium Pyrophosphate, 1 mM Sodium Orthovanadate, 0.5 mM DTT supplemented with protease inhibitor cocktail) and centrifugation at 600×*g*. The homogenates were sonicated and quantified by the Lowry method [22]. Samples were added to sample buffer (0.125 M Tris-HCl pH 6.8, 4% SDS, 20% glycerol, 10% 2-β-mercaptoetanol, 0.004% blue of bromophenol), separated by SDS–PAGE and blotted into a nitrocellulose membrane (Bio-Rad). The following primary antibodies (dilution 1:1000) were used: NAT8L (Sigma prestige antibody, HPA040677), TFAM (Santa Cruz Biotechnology, sc-166965), p-AMPK (Thr172) (Santa Cruz Biotechnology, sc-33524), AMPK (Santa Cruz Biotechnology, sc-74461), p-PDH (Ser300) (Calbiochem, AP1064), PDH (Santa Cruz Biotechnology, sc-377,092), GLUT1 (Santa Cruz Biotechnology, sc-7903), HK-2 (Abnova, H00003099-M01), p-PKM2 (Tyr105) (Cell Signaling Technology, #3827), PKM2 (Cell Signaling Technology, #4053), G6PD (Cell Signaling Technology, #D5D2), ADSL (Santa Cruz Biotechnology, sc-365,623), ACTININ (Cell signaling Technology, #3134S) and ACTIN (Sigma-Aldrich, A3853). The secondary antibodies used are Goat Anti-Rabbit IgG (H + L)–HRP Conjugate (Bio-Rad cat. #170–6515) and Goat Anti-Mouse IgG (H + L)-HRP Conjugate IgG (Bio-Rad, cat. #1706516). The signals derived from the incubation with LiteAblot® TURBO (EuroClone) were acquired using a Fluorchem imaging system (Alpha Innotech). ImageJ software was used to perform densitometry analyses.

2.5. HPLC

Metabolic analyses were performed after the deproteinization of cell samples according to a protocol suitable for obtaining protein-free extracts [23].

Briefly, cells were washed twice with ice-cold buffered PBS pH 7.4 and collected by centrifugation at 1860×*g* for 5 min at 4 °C. The cell pellets were deproteinized with the addition of a solution composed by 250 μl of ice-cold buffered PBS pH 7.40 and 750 μl of ice-cold HPLC-grade CH_3CN acetonitrile. After vigorous vortexing for 60 s, samples were centrifuged at 20,690×*g* for 10 min at 4 °C. Supernatants were collected and subjected to two chloroform washings to eliminate the organic solvent. The upper aqueous phase, obtained by centrifugation under the same conditions, was then used for the HPLC analysis and injected into the HPLC to determine concentrations of NAA, UDP-GlcNAc, acetyl-CoA, CoA, $NADP^+$, NADPH, Serine, Aspartate, Asparagine, IMP and UMP. The identification and quantification of Serine was performed using an automated precolumn sample derivatization with a mixture of ortophtalaldehyde (OPA) and 3-mercaptopropionic acid (MPA), as described elsewhere [24], whilst the other low-molecular weight compounds were analyzed and quantified according to an ion-pairing HPLC method previously set up [25]. For both analyses the HPLC equipment consisted of a Surveyor HPLC system (ThermoFisher Italia, Rodano, Milan, Italy) equipped with a highly-sensitive photodiode array detector provided with a 5 cm light path flow cell, and set up between 200 and 400 nm wavelength. Data acquisition and analyses were performed using the ChromQuest® software package provided by the HPLC manufacturer. Chromatographic separation of the various compounds was carried out using a Hypersil 250 × 4.6 mm, 5 μm particle-size column, provided with its own guard column (Thermo-Electron Italia). Species identification and quantification in cell extracts was performed by matching retention times, peak areas and absorption spectra of those of freshly prepared ultrapure standards. The concentrations of OPA-derivatized Serine, Aspartate and Asparagine were calculated at 338 nm wavelength, those of UDP-GlcNAc, acetyl-CoA, CoA, $NADP^+$, NADPH, IMP and UMP were calculated at 260 nm wavelength and those of NAA at 206 nm wavelength. In cell extracts, the total amount of proteins was determined according to the Lowry method [22]. Concentrations of low molecular weight compounds were normalized for the total cell protein concentrations and expressed as nmol/mg of proteins.

For the glutathione assay, pellets were resuspended in 200 μl of a solution composed by PBS and 0.01 M HCl (ratio 1:1). Samples were frozen and thawed in nitrogen three times. 40 μl of 25% metaphosphoric acid were added to 160 μl of samples while the remaining was used for protein quantification. After 15 min on ice samples were centrifuged at 18,620×*g* for 30 min at 4 °C. The supernatant was collected in HPLC tubes, added to 1:10 iodoacetic acid and bicarbonate powder and kept 1 h in the dark at room temperature. Sanger's reagent (EtOH/1.5% Sanger) (Sigma-Aldrich) was added 1:1 to the sample. The solution was vortexed and stored at 4 °C in the dark overnight. Samples were transferred into new tubes and centrifuged at 22,610×*g* for 20 min at 4 °C. Supernatant was collected and analyzed at HPLC, with an absorption peak of the Sanger reagent at 360 nm.

2.6. Cell proliferation assays

Cell proliferation was determined by Trypan blue exclusion test, by bromodeoxyuridine (BrdU) incorporation assay and by MTT colorimetric assay. For Trypan Blue exclusion test, cells were detached with trypsin and diluted 1:1 with a 0.08% solution of Trypan Blue (Sigma-Aldrich, T8154) for direct cell counting. For BrdU incorporation assay, cells were incubated with 10 μM BrdU (Santa Cruz Biotechnology, sc-32323) for 4 h and fixed for 30 min with 90% ethanol, 5% acetic acid, 5% water fix solution. DNA denaturation was achieved by 10 min incubation in 1 N HCl and 10 min in 2 N HCl on ice. Cells were permeabilized with PBS/0.4% Triton X-100 solution for 10 min and then blocked with PBS/3% BSA for 1 h. Anti-BrdU antibody (Santa Cruz Biotechnology, sc-32323) was incubated overnight, followed by 1 h incubation with an AlexaFluor™488 donkey anti-mouse IgG (H + L) secondary antibody (Invitrogen A21202). Nuclei were stained with 1 μg/ml of DAPI (Molecular Probes, H-3570) for 10 min. Images were obtained with a Delta Vision Restoration Microscopy System (Applied Precision) equipped with an Olympus IX70 fluorescence microscope (Olympus Italia). For cell viability evaluation by MTT colorimetric assay, cells were seeded in a 96-well plate and 100 μl of the MTT labeling reagent (Sigma-Aldrich, M2128) (0.5 mg/ml final concentration) was added per well. After 4 h incubation at 37 °C, medium was replaced with

50 μl of DMSO. Dye was solubilized in DMSO and read at 570 nm.

2.7. Seahorse analysis

Mitochondrial function and glycolytic flux were determined using a Seahorse XF96e Analyzer (Seahorse Bioscience - Agilent, Santa Clara CA, USA). At the end of the experimental time (48 h after transfection), cells were detached, counted by Trypan Blue exclusion test and re-seeded in equal number (five wells for each condition). A parallel seeding of cells was performed and the protein amount checked by the Lowry method [22] to monitor relevant changes in each experimental condition. After 8 h Cell Mito Test and Glyco Test analyses were performed.

Cell Mito Test was performed for the analysis of mitochondrial function, medium was replaced with XF test medium (Eagle's modified Dulbecco's medium, 0 mM glucose, pH = 7.4; Agilent Seahorse) supplemented with 1 mM pyruvate, 10 mM glucose and 2 mM L-glutamine. The test was performed by initially measuring the basal oxygen consumption (OCR) rate (Basal Respiration), followed by sequential injection of oligomycin (1 μM), carbonyl cyanide 4- (trifluoromethoxy) phenylhydrazone (FCCP) (1 μM) and Rotenone (0.5 μM) + Antimycin A (0.5 μM) for the OCR measurements of ATP-linked respiration and Spare Respiratory Capacity.

Glyco Test analysis was performed for the study of the glycolytic flow, medium was replaced with XF test medium (Eagle's modified Dulbecco's medium, 0 mM glucose, pH = 7.4; Agilent Seahorse) supplemented with 2 mM L-glutamine. Extracellular Acidification Rate (ECAR) was measured under basal conditions followed by the sequential addition of 10 mM glucose, 0.5 μM oligomycin, and 100 mM 2-DG.

All data were analyzed with XFe Wave software.

2.8. Cytofluorimetric analysis

Cells were incubated with MitoTracker Green (200 nM) and MitoTracker Red (200 nM) probes at 37 °C for 30 min before the end of the experimental time. Cells were trypsinized and collected in PBS for analysis. For each sample, 20,000 events were recorded in the FL-1 and FL-2 channels (for MTG and MTR, respectively) by the FACScalibur instrument. Mean fluorescence intensity was expressed as arbitrary units. MTG (M7514) and MTR (M7512) are supplied by Invitrogen.

2.9. Hexokinase and G6PD activity

Samples were lysed in a non-denaturant lysis buffer (50 mM Tris-HCl, pH 7.5, 1 mM EDTA, 150 mM NaCl, 1% NP-40, 1 mM DTT, protease inhibitor cocktail) for 30 min on ice and centrifuged at 10,000×*g* for 20 min at 4 °C. For the hexokinase activity, 50 μg of protein lysate was added to an equal volume of reaction buffer (50 mM Tris-HCl, pH 7.5, 10 mM $MgCl_2$, 0.6 mM ATP, 100 mM glucose, 0.2 mM $NADP^+$, 0.1 U/mL of glucose-6-phosphate dehydrogenase) for 30 min at 37 °C. The optical absorbance was measured at 340 nm every 15 s for 10 min with an Eppendorf BioSpectrometer®. HK activity was represented as changes in absorbance per minute (U) normalized on protein.

For the G6PD activity, 50 μg of protein lysate was added to an equal volume of reaction buffer containing 50 mM Tris, 1 mM $MgCl_2$, 100 μM $NADP^+$, pH 8.1 and 200 μM glucose-6-phosphate and/or 6-phosphogluconate. G6PD activity was calculated as the difference between the combined activity of G6PD and 6-phosphogluconate dehydrogenase (for this reaction, the buffer contains both glucose-6-phosphate and 6-phosphogluconate) and the only activity of 6-phosphogluconate dehydrogenase (buffer contains only 6-phosphogluconate). The optical absorbance was measured at 340 nm every 30 s for 6 min with an Eppendorf BioSpectrometer® G6PD activity was represented as change in absorbance per minute (U) normalized on protein.

2.10. Extracellular lactate assay

The medium was centrifugated at 600×*g* for 5 min at 4 °C, precipitated with 1:2 volume of 30% trichloroacetic acid and stored at − 20 °C for at least 1 h. Samples were centrifuged at 14,000×*g* for 20 min at 4 °C and then 10 μl of supernatant were incubated for 30 min at 37 °C in 290 μl of reaction buffer (0.2 M glycine, 0.2 M hydrazine sulphate pH 9.2 with freshly added 0.6 mg/ml NAD^+ and 17 U/ml LDH enzyme). NADH levels were evaluated by spectrophotometrically reading at 340 nm using TECAN Spectrometer and then converted to lactate concentration using the extinction coefficient of 6220 M^{-1} cm^{-1}. Values were normalized on total proteins.

2.11. Quantitative real-time PCR (RT-qPCR)

Cells were homogenized in TRItidy G (PanReact AppliChem, A4051) and then processed for the RNA extraction according to the manufacturer's instructions. Total RNA (1 μg) was used to synthesize cDNA using PrimeScript™ RT Reagent Kit (Perfect Real Time) (Takara) and RT-qPCR performed by using PowerUp SYBR Green Master Mix (Thermo Fisher Scientific) on a QuantStudio 3 Real-Time PCR system (Thermo Fisher Scientific). Primers used in the study are as follows: PPAT forward: 5′-GCGATTGAAGCACCTGTGGATG-3′, reverse: 5′-CGGTTTTTACACAGCACCTCCAC-3′; GART forward: 5′-CACCCGGTGTCGGTTTCA-3′, reverse: 5′-TTCCAGGCCAGCGTATGTTC-3′; PFAS forward: 5′-TGAGGCTATGGTGGCAGTGATG-3′, reverse: 5′-GCATAGGCTGAGATGACCAGTG-3′; ATIC forward: 5′-CCGAGAGTAAGGACACCTCCTT-3′, reverse: 5′-GGCATCTGAGATACGCCTTTGC-3′; ADSL forward: 5′-GGAGATGTGCTTCGTGTTTAG-3′, reverse: 5′-GTCGATGTTCTCCAGGTTTG -3′; HPRT1 forward: 5′-TTGGAAAGGGTGTTTATTCCTCA-3′, reverse: 5′-TCCAGCAGGTCAGCAAAGAA-3′; SLC25A12 forward: 5′-ACAAGAGTGGAAATGGAGAGGT-3′, reverse: 5′-TCTTCCGGTTATGCCCAAATG-3′; SLC25A13 forward: 5′-TGGACTGTATAGAGGTCTGTTGC-3′, reverse: 5′-CCCTCACAAAATCGTTCACTGT-3′; ACTIN forward: 5′-GGCCGAGGACTTTGATTGCA-3′, reverse: 5′-GGGACTTCCTGTAACAACGCA-3′. Data were normalized to the internal standard ACTIN and analyzed using the $2^{-\Delta\Delta Ct}$ method. The fold changes refer to the control.

2.12. Bioinformatic analysis

NAT8L expression in paired tumor and adjacent non-tumor human HCC tissues was assessed using expression data from three different datasets: The Cancer Genome Atlas Liver Hepatocellular Carcinoma (TCGA-LIHC) (50 patients), GSE82177 (8 patients) and GSE124535 (35 patients) datasets from Gene Expression Omnibus (GEO; http://www.ncbi.nlm.nih.gov/geo). NAT8L expression from GSE124535 and GSE82177 datasets was shown as Fragments Per Kilobase Million (FPKM) and DESeq normalized reads, respectively, while data from TCGA-LIHC were expressed as DESeq2 normalized reads. Statistical analysis was performed using the method indicated in the Supplementary Figs. 6A–C.

2.13. HCC human biopsies and mouse model

Human HCC samples and hepatic nodules of the mouse model of hepatocarcinogenesis were those used in our previous work [21]. Briefly, the human samples were derived from a cohort of patients with a mean age of 69.4 years. The tumor sample had a mean of 2.07 nodules and a size of 2.49 cm. In accordance with Edmonson's grade, most of the tumors were partially or moderately differentiated. The use of clinical samples was approved by the ethics committee of Regina Elena Tumor Institute. Hepatic nodules of the mouse model of hepatocarcinogenesis were from mice intraperitoneally injected with Diethylnitrosamine (DEN) and fed with Choline deficient diet (CDD). Reference control group was intraperitoneally injected with saline solution and fed standard pellets. The murine experimentation was performed in accordance

with the regulations for the care of human animals and after approval by the Italian Ministry of Welfare Committee and the Institutional Animal Care and Use Committee of the University of Rome 'Tor Vergata' (Italy).

Human and mouse samples were lysed in the lysis buffer described above and homogenized using Ultra-Turrax T25 for 30 times on ice. Centrifugation at 10,000×*g* for 20 min at 4 °C allows the removal of any debris. The supernatant was further sonicated, quantified by Lowry method [22] and finally combined with the sample buffer described above.

2.14. Data analysis

Data analysis derived from at least 3 independent experiments. The results are presented as means ± SD. Statistical analysis was carried out through GraphPad Prism 7 software using Student's t-test for comparisons of only two variables, one-way ANOVA with Tukey post hoc for multiple comparisons and Wilcoxon matched pairs test for HCC biopsies and mouse nodules. Results were considered statistically significant at $p \leq 0.05$.

3. Results

3.1. NAT8L downregulation promotes the proliferation of hepatocarcinoma cells

To test how NAT8L contributes to cancer metabolic reprogramming in HCC, we knocked down its expression by using two different siRNA sequences (NAT8L KD1 and KD2) (Fig. 1A) that efficiently decreased NAA levels (Fig. 1B). The analysis of proliferation by the direct cell counting (Fig. 1C), BrdU incorporation (Fig. 1D) and MTT cell viability assay (Supplementary Fig. 1A) showed that the downregulation of NAT8L increases the proliferation rate of HepG2 cells. The same result was obtained in another hepatocarcinoma cell line, HuH7 cells, following NAT8L downregulation (Fig. 1E). On the contrary, a reduction of HepG2 cell proliferation was observed upon overexpression of NAT8L (Supplementary Fig. 1B-F), suggesting an association between HCC cell line proliferation rate and NAT8L expression levels.

Then we focused on the metabolic trait underlying the increase in proliferation, a typical feature of transformed cells. As NAT8L is a mitochondrial enzyme that uses acetyl-CoA as substrate, thus affecting its availability for bioenergetics, we verified the effects of NAT8L downregulation on mitochondrial oxidation. Analysis performed by the Seahorse analyzer revealed a slight decrease in mitochondrial respiration (Fig. 1F) and ATP production (Fig. 1G) in NAT8L-silenced cells. These results were not associated with a bioenergetic deficit or dysfunctional mitochondria, as demonstrated by the unaltered levels of the active phospho-AMPK form (Supplementary Fig. 1G), MitoTracker Red/MitoTracker Green ratio (Supplementary Fig. 1H) and Spare Respiratory Capacity (Fig. 1H), but instead to a decrease in mitochondrial mass as indicated by the low levels of Transcription Factor A Mitochondrial (TFAM) expression (Fig. 1I) and MitoTracker Green fluorescence (Supplementary Fig. 1I).

3.2. Mitochondrial metabolism and glutamine oxidation support HepG2 proliferation in NAT8L-silenced cells

We validated the relevance of mitochondrial bioenergetics in NAT8L-silenced cells by monitoring cell growth in the presence of the ATP synthase inhibitor oligomycin. Fig. 2A showed that the treatment decreased the proliferation of NAT8L-silenced cells abolishing the proliferative advantage imposed by NAT8L downregulation. Oligomycin treatment was paralleled by an increase in lactate production (Supplementary Fig. 2A), indicative of a higher glycolytic rate for energy supply, and with an increase in the activated phospho-AMPK form, as a signaling event of the impaired energy production at the level of mitochondria (Fig. 2B). It is important to notice that the phospho-AMPK levels were higher in NAT8L-silenced cells indicating they highly rely on mitochondrial bioenergetics.

In proliferating cells, mitochondrial respiration is not only necessary for ATP production but also nucleotides synthesis. Consistently, the oxidation of coenzymes by the mitochondrial respiratory chain is indispensable for redox homeostasis required for aspartate synthesis. Exogenous pyruvate can be experimentally used to overcome redox unbalance in cells having less efficient mitochondria [10]. Under our experimental conditions, treatment with pyruvate does not affect the proliferation of NAT8L-silenced cells, while it significantly accelerated cell growth in scramble (SCR) cells (Fig. 2C). This result suggests that redox state settled by NAT8L silencing contributes to promote cell proliferation. However, the treatment with oligomycin is detrimental for both SCR and NAT8L-silenced cells even in the presence of pyruvate, here used to compensate defective redox capability of the respiratory chain following inhibition of mitochondrial ATP synthase (Fig. 2D). Altogether, these results demonstrate that NAT8L downregulation assures the proper redox homeostasis required to increase the proliferation rate, which strictly depends on the bioenergetic supply provided by mitochondria.

The relevance of mitochondrial bioenergetics in promoting the proliferation of NAT8L-silenced cells prompted us to evaluate which metabolic fuel mainly contributed to this phenotype. We first verified the involvement of glucose-derived pyruvate by inhibiting glycolysis with 2-deoxyglucose (2-DG). Direct cell counting demonstrated that glucose utilization is necessary for the proliferative advantage of NAT8L-silenced cells (Fig. 2E). Nevertheless, we determined an increased acetyl-CoA/CoA ratio (Supplementary Fig. 2B), which is consistent with increased levels of the inhibitory phosphorylation of pyruvate dehydrogenase (p-PDH Ser300) (Fig. 2F). This result revealed that pyruvate is less efficiently oxidized at the mitochondrial level and cannot account for the increased proliferation rate upon NAT8L silencing. Then, considering the relevance of glutamine in cancer mitochondrial metabolism, we cultured cells into a glutamine-free medium or in the presence of the glutaminase inhibitor BPTES. Fig. 2G shows that the proliferation of cells downregulating NAT8L was significantly decreased in the absence of glutamine, even in comparison with the inhibition observed for scramble cells. The same result was obtained by BPTES (Fig. 2G), finally demonstrating the need for fuelling glutamine oxidation for the proliferative advantage of NAT8L-silenced cells.

3.3. Pentose phosphate pathway activation is essential for increased proliferation of NAT8L-silenced cells

To elucidate the role of glucose metabolism in NAT8L-silenced cells, we assessed critical steps of the glycolytic pathway. We revealed an upregulation of the glucose transporter GLUT1 (Fig. 3A) associated with increased expression and activity of hexokinase-2 (HK-2) (Fig. 3A and Supplementary Fig. 3A, respectively), indicative of enhanced glucose uptake and phosphorylation. However, the increased upstream flux of glycolysis was not supported by the downstream reactions of aerobic glycolysis, as demonstrated by both the increased inhibitory phosphorylation of Pyruvate kinase isozyme M2 (p-PKM2 Tyr105) (Fig. 3A), the latter regulatory enzyme of the glycolytic rate, and by unchanged levels of extracellular lactate (Fig. 3B) and acidification rate (ECAR) (Supplementary Fig. 3B). This picture resembles a typical metabolic adaptation of cancer cells funnelling glycolytic intermediates in branching metabolic pathways. We excluded a significant contribution of the hexosamine and serine biosynthetic pathways due to unaltered levels of the UDP-N-acetylglucosamine (UDP-GlcNac) and serine (Supplementary Figs. 3C–D). Conversely, we observed the activation of the pentose phosphate pathway (PPP), as demonstrated by the reduced $NADP^+$/NADPH ratio (Fig. 3C) coupled with increased expression and activity of the rate-limiting enzyme glucose-6-phosphate dehydrogenase (G6PD) (Fig. 3D and E). The prominent role played by this pathway was demonstrated by the treatment with the PPP inhibitor 6-

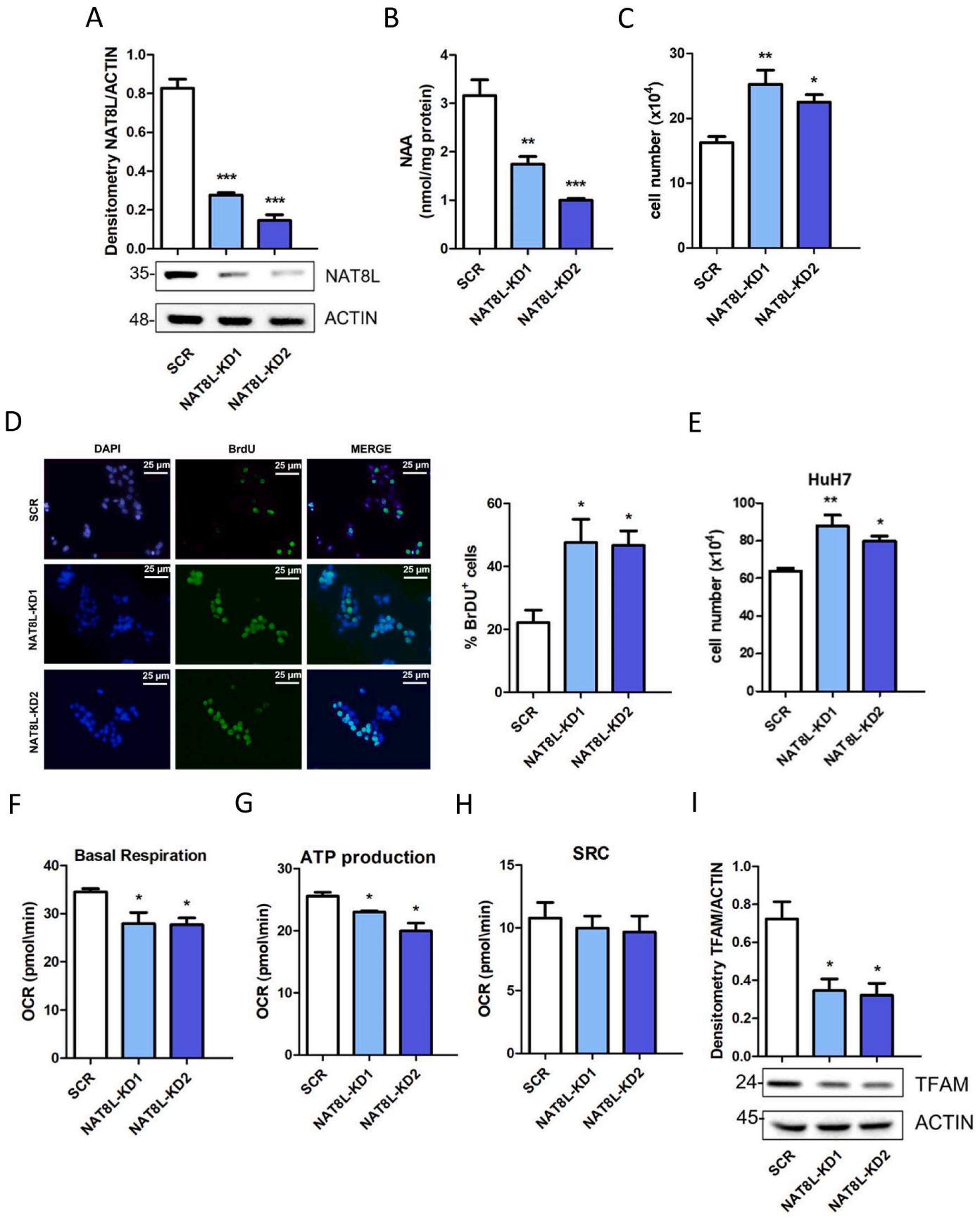

(caption on next page)

Fig. 1. NAT8L downregulation promotes proliferation of hepatocarcinoma cells. (**A**) Representative Western blot of NAT8L silencing in HepG2 cells (bottom panel). ACTIN was used as loading control. The upper bar graph refers to the densitometry analysis (n = 3; ***$P < 0.001$ vs SCR). (**B**) Determination of NAA levels performed in HepG2 cells by HPLC analysis (n = 3; **$P < 0.01$, ***$P < 0.001$ vs SCR). (**C**) Cell proliferation evaluated in HepG2 cells by Trypan blue direct cell counting (n = 6; *$P < 0.05$, **$P < 0.01$ vs SCR). (**D**) Cell proliferation evaluated in HepG2 cells by BrdU incorporation assay. Bar graph refers to the percentage of BrdU-positive cells (n = 3; *$P < 0.05$ vs SCR). (**E**) HuH7 proliferation evaluated by Trypan blue direct cell counting assay (n = 6; *$P < 0.05$, **$P < 0.01$ vs SCR). Bar graph obtained from Seahorse analysis in HepG2 cells and representing (**F**) basal respiration (n = 3; *$P < 0.05$ vs SCR), (**G**) ATP production (n = 3; *$P < 0.05$ vs SCR), (**H**) spare respiratory capacity (SRC) (n = 3). (**I**) Representative Western blot showing levels of TFAM as a marker of mitochondrial mass in comparison with ACTIN used as the loading control (bottom panel). The upper bar graph refers to the densitometry analysis (n = 3 *$P < 0.05$ vs SCR).

aminonicotinamide (6-AN) (Fig. 3F) and by G6PD silencing. The decrement of G6PD expression after RNAi (Supplementary Fig. 3E) specifically inhibited the proliferative advantage of NAT8L-silenced cells measured either with the Trypan Blue vital dye (Fig. 3G) or by the MTT assay (Supplementary Fig. 3F). Cancer cells experience increased oxidative stress due to intense proliferation and NADPH produced by PPP is an essential source of reducing equivalents used by cells to convert oxidized glutathione (GSSG) to glutathione (GSH), an abundant redox buffer. In agreement with PPP activation, we revealed a more efficient antioxidant system in NAT8L-silenced cells in terms of increased levels of GSH (Supplementary Fig. 3G).

3.4. Cytosolic aspartate availability supports de novo purine synthesis and proliferation of NAT8L-silenced cells

PPP is also at the centre stage of high proliferating cells by supplying ribose for nucleotide biosynthesis. To test how the metabolism of the NAT8L-silenced cells adapted to the upregulation of PPP, we quantified critical intermediates of the synthesis of the nucleobases using HPLC analysis. While a slight increase in uridine monophosphate (UMP) levels was observed in NAT8L-silenced cells, we measured a significant enrichment of the common precursor of purines inosine monophosphate (IMP) (Fig. 4A). Hereafter, we have specifically assessed the role of purines in our system taking into account that their production is necessary coupled with pyrimidine synthesis to promote proliferation. NAT8L-silenced cells showed the upregulation of Phosphoribosyl Pyrophosphate Amidotransferase (PPAT), Phosphoribosylglycinamide Formyltransferase (GART), Phosphoribosylformylglycinamidine Synthase (PFAS) and Adenylosuccinate Lyase (ADSL) (Fig. 4B): these are the enzymes responsible for consecutive reactions necessary for the conversion of Phosphoribosyl pyrophosphate (PRPP) into the IMP and thus involved in the *de novo* purine synthesis. On the contrary, RT-qPCR analysis revealed that the expression of the key component of the purine salvage pathway Hypoxanthine Phosphoribosyltransferase 1 (HPRT1) was not modulated (Supplementary Fig. 4A). The abrogation of the *de novo* purine synthesis by the inhibitor 6-mercaptopurine (6-MP) (Fig. 4C; Supplementary Fig. 4B) and by silencing the enzymes PPAT (Fig. 4D; Supplementary Figs. 4C–D) and ADSL (Supplementary Figs. 4E–G), demonstrated that this pathway guarantees the increased proliferative capacity of NAT8L-silenced cells.

Nucleotide synthesis in proliferating cells is limited by cytosolic aspartate levels, which can depend on mitochondrial supply [10,26,27] or on exogenous intake [12,13]. Under our experimental condition, mitochondrial aspartate represents a substrate of NAT8L and can be more available for alternative anabolic pathways in NAT8L-silenced cells. HPLC analysis revealed that the concentration of aspartate was not changed in NAT8L-silenced cells (Fig. 4E), whereas the asparagine levels, the synthesis of which is strictly dependent on cytosolic aspartate availability, were significantly increased (Fig. 4F). Since aspartate is poorly cell-permeable, the aspartate export from mitochondria becomes indispensable for nucleotide synthesis and in turn for proliferation [26]. Considering this, the role of mitochondrial aspartate carriers appears fundamental to guaranteeing the extrusion of aspartate into the cytosol, where nucleotide synthesis occurs. To verify whether the effects on proliferation were due to aspartate shuttling from mitochondria to cytosol, we monitored the proliferation of NAT8L-silenced cells upon downregulation of SLC25A13, the most expressed mitochondrial aspartate exporter in our cells (Supplementary Fig. 4H). The results indicated that restricting aspartate to mitochondria by SLC25A13 downregulation (Supplementary Fig. 4I) prevents the proliferative capability of NAT8L-silenced cells (Fig. 4G and Supplementary Fig. 4J). Interestingly, the outflow of aspartate from mitochondria also signals the activation of PPP and *de novo* purine synthesis in NAT8L-silenced cells. In fact, SLC25A13 silencing dampened the upregulation of G6PD and ADSL expression observed in the absence of NAT8L (Fig. 4H). Together these data demonstrate that the increased proliferation of NAT8L-silenced cells relies on the activation of *de novo* nucleotide synthesis boosted by cytosolic aspartate availability deriving from the impairment of NAT8L mitochondrial activity.

3.5. NAT8L downregulation also enhances proliferation rate in immortalized human hepatocytes HuS-E/2 by activating PPP and purine biosynthesis

To identify NAT8L downregulation as a signature that correlates with cell transformation, we performed key experiments in the immortalized human hepatocytes HuS-E/2 cell line. We confirmed that the absence of NAT8L (Fig. 5A) and the decrease of NAA levels (Fig. 5B) promoted cell proliferation (Fig. 5C; Supplementary Fig. 5A). We corroborated that NAT8L downregulation is associated with a redirection of glucose flux into the PPP as demonstrated by increased levels of PKM2 inhibitory phosphorylation (Supplementary Fig. 5B), G6PD expression and activity (Fig. 5D and E), and reduction of the $NADP^+$/NADPH (Supplementary Fig. 5C). To confirm the importance of PPP in maintaining the proliferative capacity of HuS-E/2 cells, we used 2-DG and 6-AN, which recapitulated the loss of the proliferative advantage of NAT8L-silenced cells after the inhibition of glucose utilization (Supplementary Figs. 5D–E). In parallel, we confirmed that mitochondrial anaplerosis elicited by glutaminolysis is fundamental in NAT8L-silenced cells, as their proliferative capacity was restricted by BPTES treatment (Fig. 5F). Also, the metabolic rewiring elicited by NAT8L downregulation in HuS-E/2 led to an increase in the levels of the purine intermediate IMP, the pyrimidine intermediate UMP (Fig. 5G) and of the enzymes involved in the purine synthesis (Fig. 5H). We targeted this biosynthetic pathway using the inhibitor 6-MP (Fig. 5I; Supplementary Fig. 5F) and downregulating PPAT (Fig. 5J; Supplementary Figs. 5G–H), demonstrating the inability of NAT8L-silenced cells to increase proliferation.

3.6. NAT8L downregulation is intimately connected with HCC in patients and mice

We finally investigated the *in vivo* significance of NAT8L expression in HCC. The analysis of TCGA and GEO datasets was used to verify changes in the expression of NAT8L gene in different HCC cohorts. We observed that NAT8L mRNA levels were not significantly affected in HCC samples compared to paired non-tumor liver specimens. These results suggest that NAT8L expression is not regulated at the transcription level in HCC (Supplementary Figs. 6A–C). Therefore, we monitored the protein levels of NAT8L in tumor biopsies (T) and corresponding non-tumor (NT) portions in a cohort of HCC patients and in a mouse model of induced HCC, available in our laboratory. Western Blotting analysis evidenced that the protein content of NAT8L was significantly decreased in human HCC biopsies (Fig. 6A and B and Supplementary

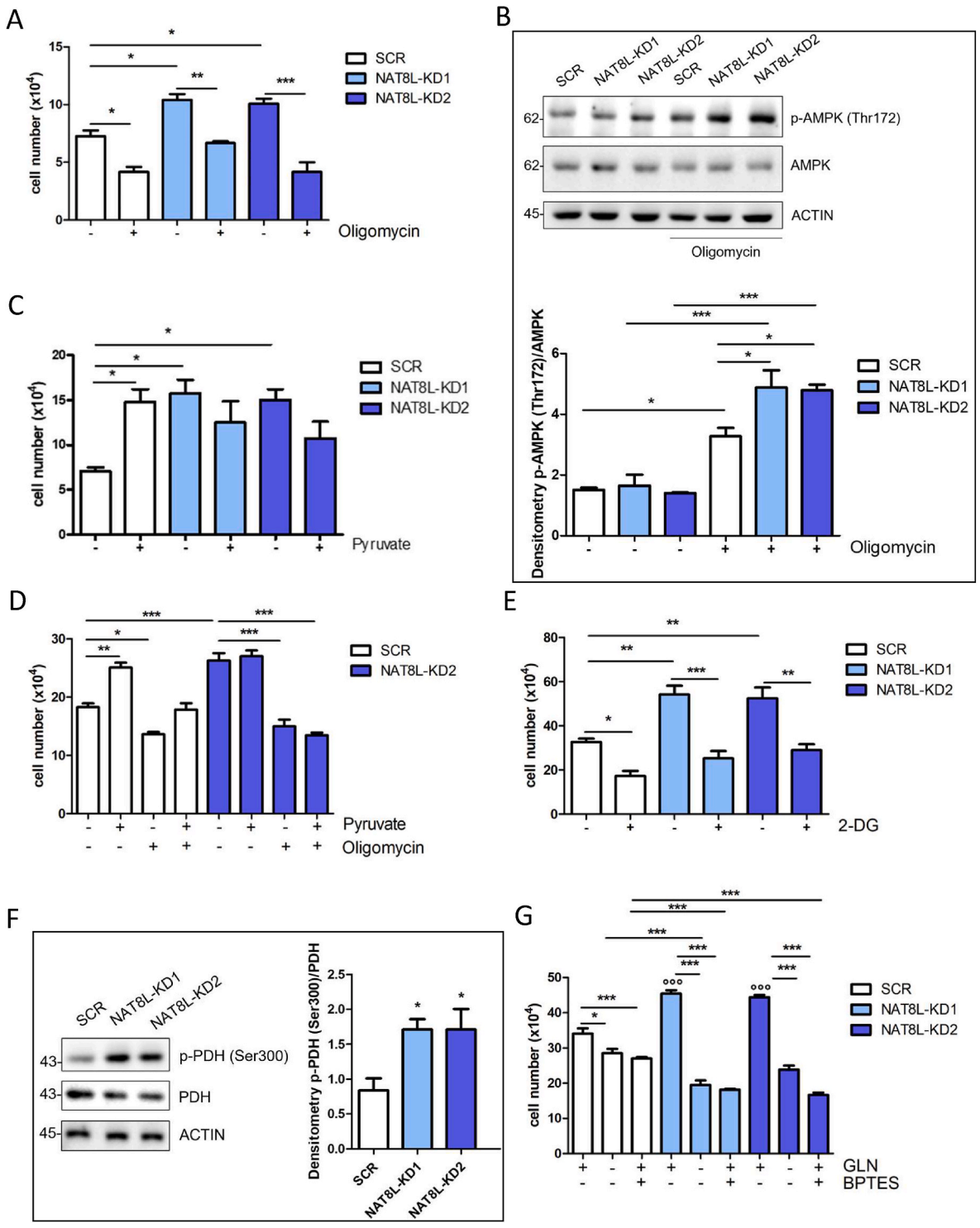

Fig. 2. Mitochondrial metabolism and glutamine oxidation support proliferation in NAT8L-silenced cells. (**A**) Cell proliferation evaluated by Trypan blue direct cell counting upon HepG2 treatment with 100 nM oligomycin for 24 h (n = 3; *$P < 0.05$, **$P < 0.01$, ***$P < 0.001$ as indicated). (**B**) Representative Western blot analysis of AMPK Thr172 phosphorylation upon HepG2 treatment with 100 nM oligomycin for 24 h. ACTIN was used as loading control. The bar graph refers to the densitometry analysis (n = 3; *$P < 0.05$, ***$P < 0.001$ as indicated). (**C**) Cell proliferation was evaluated by Trypan blue direct cell counting assay upon treatment of HepG2 cells with 1 mM sodium pyruvate (48 h) (n = 4; *$P < 0.05$ as indicated). (**D**) Cell proliferation of HepG2 cells evaluated by Trypan blue direct cell counting assay upon 1 mM sodium pyruvate (48 h) and 100 nM oligomycin (24 h) co-treatment (n = 3; *$P < 0.05$, **$P < 0.01$, ***$P < 0.001$ as indicated). (**E**) Cell proliferation evaluated by Trypan Blue direct cell counting assay upon HepG2 treatment with 10 mM 2-DG (24 h) (n = 4; *$P < 0.05$, **$P < 0.01$, ***$P < 0.001$ as indicated). (**F**) Representative Western blot analysis of PDH Ser300 phosphorylation in HepG2 cells. ACTIN was used as loading control. The bar graph refers to the densitometry analysis (n = 3 *$P < 0.05$ *vs SCR*). (**G**) Cell proliferation evaluated by Trypan blue direct cell counting assay upon treatment of HepG2 cells with a glutamine-free medium or 20 μM BPTES (24 h) (n = 4; *$P < 0.05$, ***$P < 0.001$ as indicated; °$P < 0.001$ *vs SCR*).

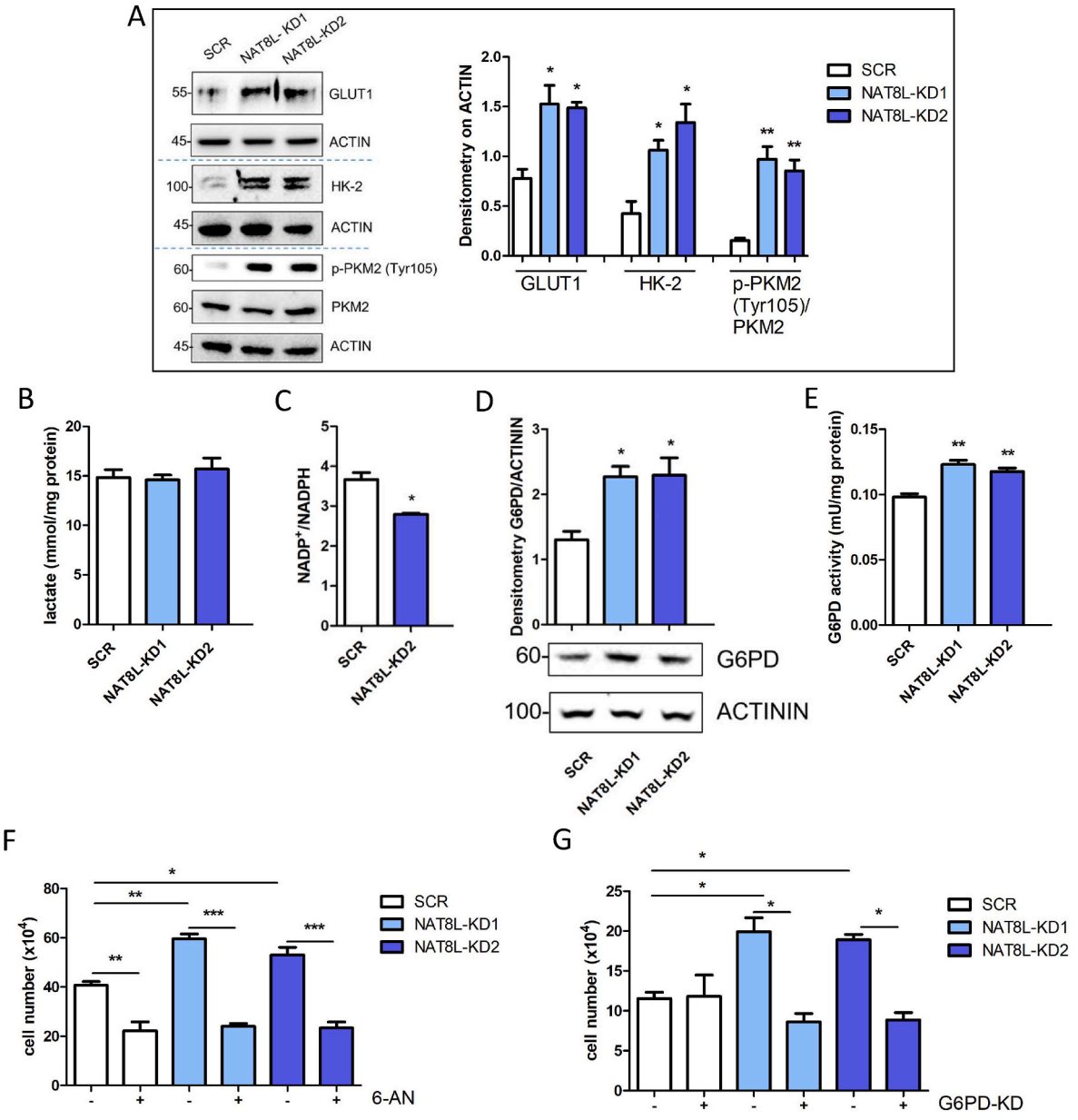

Fig. 3. Pentose phosphate pathway activation is essential for increased proliferation of NAT8L-silenced cells. (**A**) Western blot analysis of GLUT1, HK-2 and PKM2 Tyr105 phosphorylation in HepG2 cells. ACTIN was used as the loading control. Bar graph on the right refers to the densitometry analysis (n = 3; *$P < 0.05$, **$P < 0.01$ *vs SCR*). (**B**) Spectrophotometric analysis of extracellular lactate content in HepG2 cells. Lactate concentration was normalized on total protein levels (n = 3). (**C**) Determination of $NADP^+$/NADPH performed in HepG2 cells by HPLC analysis (n = 3; *$P < 0.05$ *vs SCR*). (**D**) Representative Western blot of G6PD in HepG2 cells (bottom panel). ACTININ was used as the loading control. The upper bar graph refers to the densitometry analysis (n = 3; *$P < 0.05$ *vs SCR*). (**E**) Spectrophotometric analysis of G6PD activity in HepG2 cells normalized on total protein levels (n = 3; **$P < 0.01$ *vs SCR*). (**F**) Cell proliferation evaluated by Trypan blue direct cell counting assay upon treatment of HepG2 cells with 15 μM 6-AN (24 h) (n = 3; *$P < 0.05$, **$P < 0.01$, ***$P < 0.001$ as indicated). (**G**) Cell proliferation evaluated by Trypan blue direct cell counting assay upon G6PD downregulation in HepG2 cells (n = 3; *$P < 0.05$ as indicated).

Fig. 6D) and nodules deriving from the HCC mouse model (Fig. 6C and D). Consistently with data obtained *in vitro*, the decreased expression of NAT8L was mainly associated with an increase in the levels of G6PD and ADSL. These data strengthen the functional link of NAT8L metabolism with the PPP and purine biosynthetic pathways in HCC.

4. Discussion

Cancer cells exploit metabolic rearrangements to proliferate and adapt to environmental pressures in the tumor microenvironment. Many metabolic pathways underused by differentiated cells become fundamental for sustaining cancer cell fitness. While in normal physiological conditions, the salvage pathway is sufficient to maintain the nucleotide pools [28,29], malignant transformation and uncontrolled cell growth necessitate activating *de novo* synthesis to satisfy the increased nucleotide demands [28,30]. Accordingly, NAT8L-silenced HepG2 cells show increased proliferation and high levels of nucleobases precursors, particularly the purine precursor IMP. We suggest that also pyrimidine synthesis is elevated in our conditions to promote proliferation, as indicated by the significant increase of UMP in NAT8L-silenced HuS-E/2 cells. Purine and pyrimidine biosynthesis consists of several enzymatic reactions entailing an ample supply of energy and amino acids. In this scenario, an essential contribution is played by mitochondria for their ability to generate a high amount of ATP as well as aspartate, which

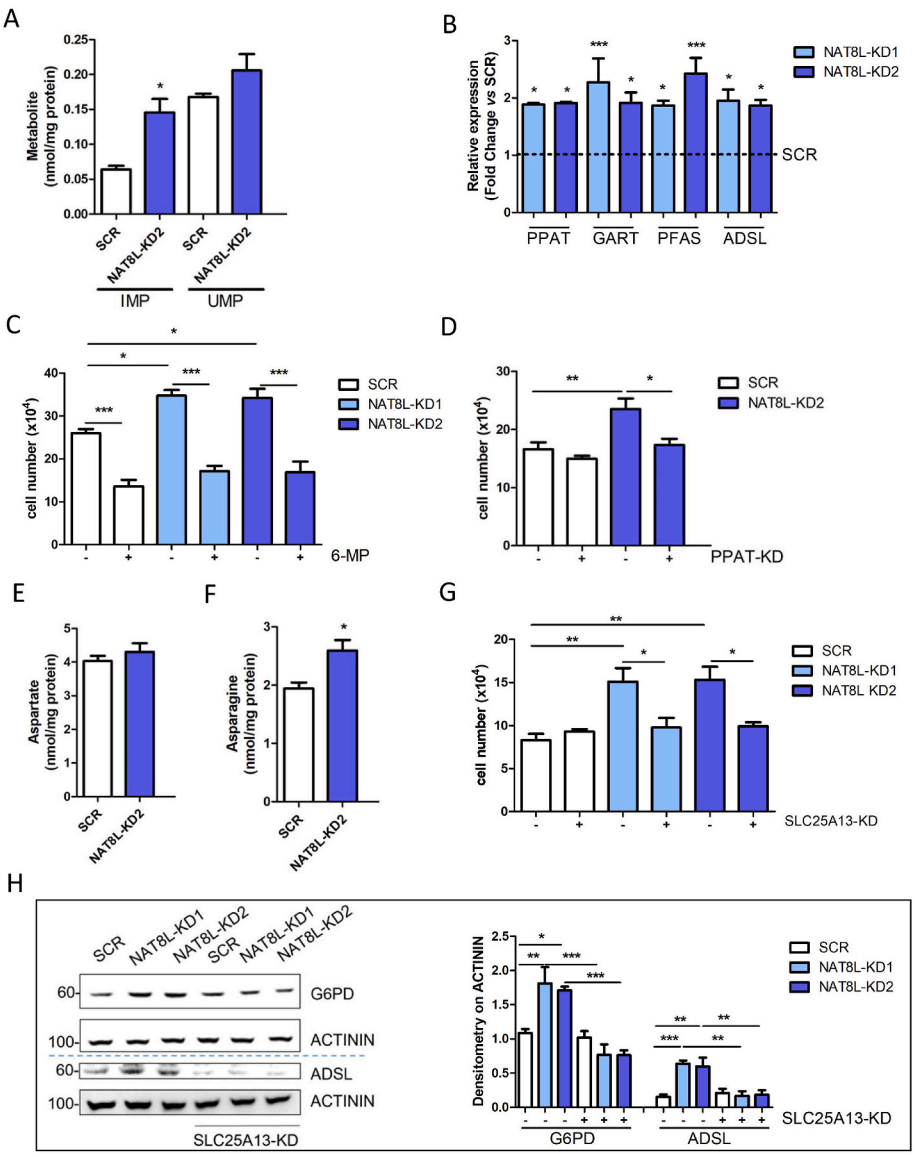

Fig. 4. Cytosolic aspartate availability supports *de novo* purine synthesis and proliferation of NAT8L-silenced cells. (**A**) Determination of IMP and UMP levels performed in HepG2 cells by HPLC analysis. (n = 3; *$P < 0.05$ vs. SCR*). (**B**) RT-qPCR analysis of PPAT, GART, PFAS and ADSL in HepG2 cells by using ACTIN as reference control (n = 3; *$P < 0.05$, ***$P < 0.001$ vs SCR*). (**C**) Cell proliferation evaluated by Trypan Blue direct cell counting assay upon HepG2 treatment with 80 μM 6-MP (24 h) (n = 4; *$P < 0.05$, ***$P < 0.001$* as indicated). (**D**) Cell proliferation evaluated by Trypan blue direct cell counting assay upon PPAT downregulation in HepG2 cells (n = 4; *$P < 0.05$, **$P < 0.01$* as indicated). (**E**) Determination of aspartate levels performed in HepG2 cells by HPLC analysis (n = 3). (**F**) Determination of asparagine levels performed in HepG2 cells by HPLC analysis (n = 3; *$P < 0.05$ vs SCR*). (**G**) Cell proliferation evaluated by Trypan blue direct cell counting assay upon SLC25A13 downregulation in HepG2 cells (n = 3; *$P < 0.05$, **$P < 0.01$* as indicated). (**H**) Representative Western blot analysis of G6PD and ADSL upon SLC25A13 downregulation in HepG2 cells. ACTININ was used as the loading control. Bar graph refers to the densitometry analysis (n = 3; *$P < 0.05$, **$P < 0.01$, ***$P < 0.001$* as indicated).

represents a limiting amino acid for nucleotide biosynthesis and tumor growth [10,31]. In fact, the mitochondrial electron transport chain is also fundamental for providing electron acceptors for aspartate synthesis in proliferating cells [10].

Our data demonstrate that NAT8L downregulation confers a proliferative advantage to HepG2 and HuS-E/2 cells, promoting an increased availability of cytosolic aspartate. Our results indicate that the pool of mitochondrial aspartate not used in NAA synthesis due to NAT8L deficiency is extruded from mitochondria and acts as a pro-proliferative signal, boosting the PPP and *de novo* purine synthesis to foster proliferation. Consistently, the depletion of the mitochondrial aspartate exporter SLC25A13, which would limit the increase in cytosolic aspartate availability, hindered the proliferative capacity of NAT8L-silenced cells impairing the induction of PPP and purine biosynthesis. Analogously, the downregulation of the paralogue aspartate transporter SLC25A12 in HCC also hampers the supply of cytosolic aspartate for nucleotide biosynthesis [27]. The mitochondrial aspartate efflux is fundamental for the cytosolic redox balance participating in the malate-aspartate shuttle (MAS). In particular, the activity of SLC25A13 is important especially in the MAS of the liver [32]. The increased levels of cytosolic aspartate mediated by SLC25A13 are likely to enhance MAS activity in our conditions thus contributing to regenerate cytosolic NAD^+, necessary for augmenting glycolytic flux.

As a proxy indicator of increased cytosolic aspartate availability, we observed an increased level of asparagine, the synthesis of which exclusively occurs in the cytoplasm and relies on glutamine availability as the amino group donor. Asparagine also plays a non-metabolic role in cancer cells by activating mTORC signaling and serine uptake necessary for the coordination of protein and nucleotide synthesis in response to increased anabolic demands of highly proliferating cells [33,34]. Therefore, in our experimental conditions, increased asparagine synthesis may even represent an integral part of the new metabolic scenario established by NAT8L downregulation, by contributing to the increased biosynthesis of nucleotide.

Analogously to nucleotide biosynthesis [10], asparagine synthesis also depends on redox homeostasis maintained by mitochondrial respiration, which is required to yield aspartate [34]. In our conditions, mitochondria of NAT8L-silenced cells guarantee an adequate redox state since no proliferative changes were obtained after using pyruvate, which is known to recover aspartate biosynthesis in cells with inefficient respiration by supplying electron acceptors following reduction by lactate dehydrogenase [10]. Moreover, mitochondrial metabolism, not aerobic glycolysis, met the novel bioenergetic requirements necessary for promoting cell growth without NAT8L. Indeed, the inhibition of ATP

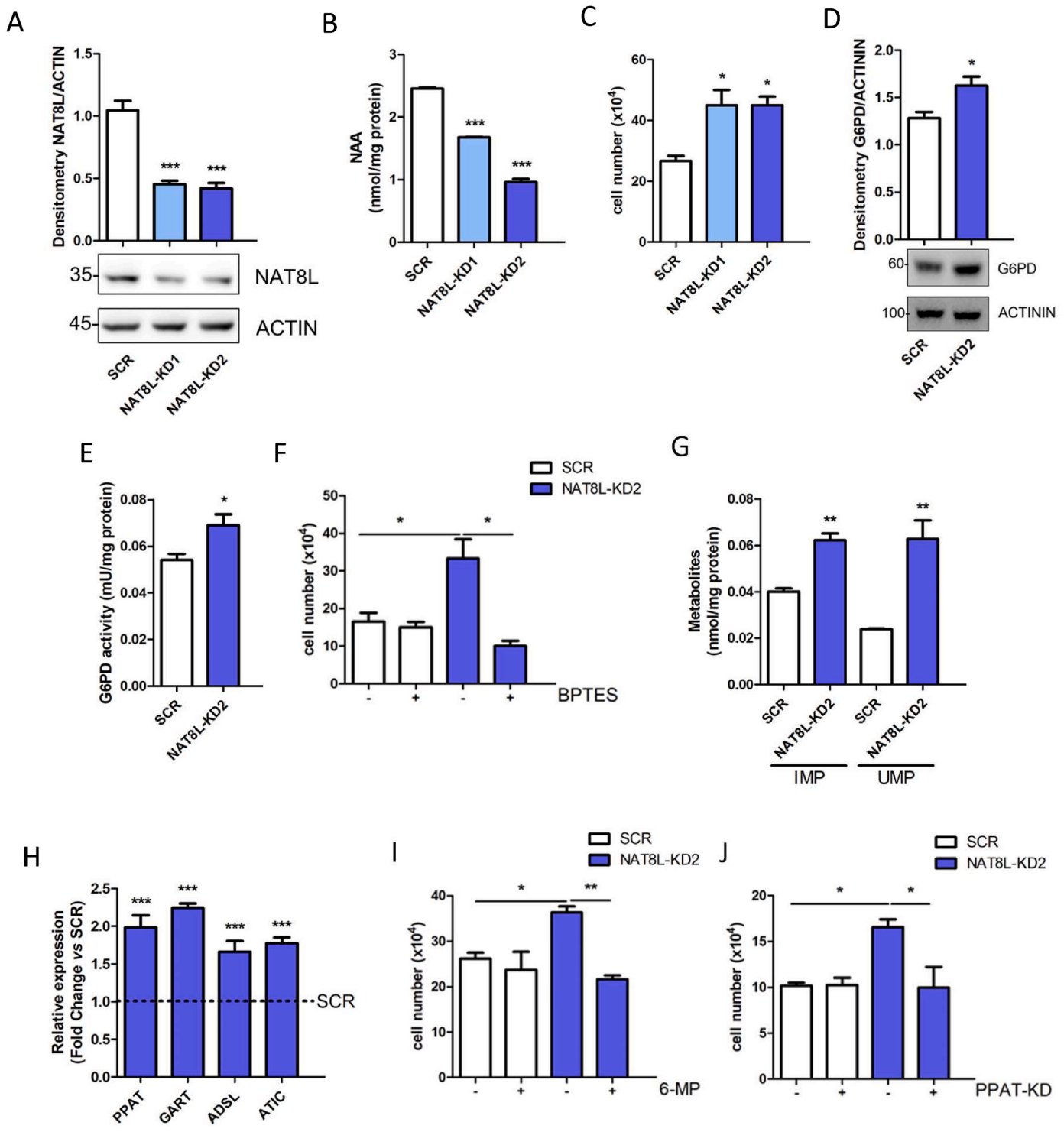

Fig. 5. NAT8L downregulation enhances proliferation rate in immortalized human hepatocytes HuS-E/2 by activating PPP and purine biosynthesis. (**A**) Representative Western blot of NAT8L silencing in HuS-E/2 cells (bottom panel). ACTIN was used as the loading control. The upper bar graphs refer to the densitometry analysis (n = 3; ****P < 0.001 vs SCR*). (**B**) Determination of NAA levels in HuS-E/2 cells performed by HPLC analysis (n = 3; ****P < 0.001 vs SCR*). (**C**) Cell proliferation evaluated by Trypan blue direct cell counting in HuS-E/2 cells (n = 3; **P < 0.05 vs SCR*). (**D**) Representative western of G6PD expression in HuS-E/2 cells (bottom panel). ACTININ was used as loading control. The upper bar graph refers to the densitometry analysis (n = 3; **P < 0.05 vs SCR*). (**E**) Spectrophotometric analysis of G6PD activity in HuS-E/2 cells, normalized on total protein levels (n = 3; **P < 0.05 vs SCR*). (**F**) Cell proliferation evaluated by Trypan blue direct cell counting assay upon treatment of HuS-E/2 cells with 20 μM BPTES (24 h) (n = 3; **P < 0.05 vs SCR*). (**G**) Determination of IMP and UMP levels measured in HuS-E/2 cells by HPLC (n = 3; ***P < 0.01 vs SCR*). (**H**) RT-qPCR analysis of PPAT, GART, ADSL and ATIC genes in HuS-E/2 cells using ACTIN as reference control (n = 3; ****P < 0.001 vs SCR*). (**I**) Cell proliferation evaluated by Trypan Blue direct cell counting assay upon treatment of HuS-E/2 cells with 80 μM 6-MP (24 h) (n = 3; **P < 0.05, **P < 0.01* as indicated). (**J**) Cell proliferation evaluated by Trypan blue direct cell counting assay upon PPAT downregulation in HuS-E/2 cells (n = 4; **P < 0.05 vs SCR*).

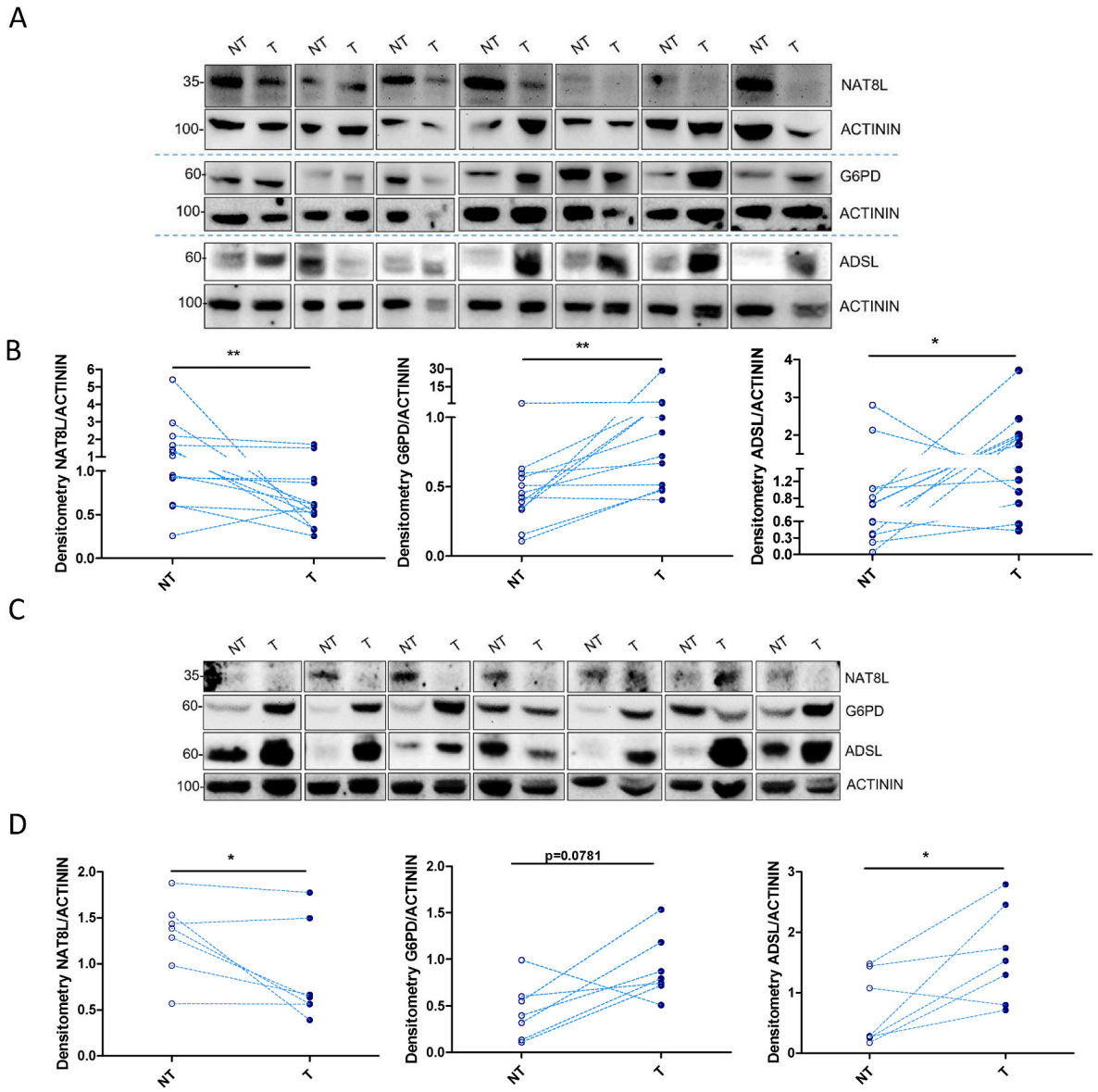

Fig. 6. NAT8L downregulation is intimately connected with HCC from patients and mice. (**A**) Representative Western blot analysis of NAT8L, G6PD and ADSL levels in tumoral (T) and respective non-tumoral (NT) counterparts in human HCC biopsies. ACTININ was used as the loading control. (**B**) The graphs refer to the densitometry of NAT8L, G6PD and ADSL in Fig. 6A and Fig. S6D and normalized on ACTININ (n = 13; *$P < 0.05$, **$P < 0.01$ *vs NT*). (**C**) Representative Western blot analysis of NAT8L, G6PD and ADSL levels in tumoral (T) and respective non-tumoral (NT) counterparts of HCC mouse model. ACTININ was used as the loading control (n = 7). (**D**) The graph refers to the densitometry of NAT8L, G6PD and ADSL on ACTININ (n = 7; *$P < 0.05$ *vs NT*).

synthase was paralleled by an increase in the glycolytic rate in terms of lactate production as a compensatory mechanism, but this was not sufficient for avoiding growth arrest and AMPK activation due to energetic stress.

Cancer cells massively utilize glutamine as a source of both carbon and nitrogen for anabolic reactions and as a substrate of the Krebs' cycle following conversion in glutamate and then 2-oxoglutarate. Considering the active synthesis of purines observed in NAT8L-silenced cells, glutamine is necessarily employed as a nitrogen donor independently of its oxidation. However, the glutaminase inhibition clarified that glutaminolysis is required to sustain the proliferative advantage by mitochondrial anaplerosis. The relevance of glutamine is well established in HCC metabolism, where it can promote cell survival upon glucose starvation [35]. Moreover, increased glutamine anaplerosis accompanies lipotoxicity, and these represent hepatic manifestations of the HCC risk factor NASH [36]. In cancer cells, glutamine is also essential for generating aspartate to employ in nucleotide biosynthesis. Aspartate administration was shown to rescue the S-phase arrest of KRas-driven cancer cells facing glutamine withdrawal [37]. Glutamine-dependent aspartate is typically formed by glutamate-oxaloacetate transaminases, which produce aspartate, transferring the amino group from glutamine-derived glutamate to oxaloacetate with the release of 2-oxoglutarate. Nevertheless, when the utilization of pyruvate in the Krebs' cycle is hindered, as observed in NAT8L-silenced HepG2 cells that display PDH inhibition, glutamine also constitutes the carbon skeleton for aspartate representing the primary source of mitochondrial 2-oxoglutarate and thus oxaloacetate. A direct connection between glutamine and cytosolic aspartate availability was highlighted in cells depleted for the mitochondrial aspartate-glutamate transporter SLC25A12, which undergo cell death after inhibiting glutaminolysis by CB-839. Cell survival was rescued by the administration of exogenous aspartate [26]. All this evidence supports that glutamine addiction of NAT8L-silenced cells may satisfy multiple metabolic requirements necessary to boost cell proliferation.

Besides assuring amino acids for constructing nitrogenous bases, cancer cells need to generate ribose moiety to engage in nucleotide biosynthesis. Consistently, the metabolic setting imposed by NAT8L silencing also consists of a prominent activation of G6PD, which provides ribose-5-phosphate and NADPH, catalyzing the rate-limiting step in the oxidative branch of PPP. The activation of the PPP is one of the typical metabolic signatures of cancer cells. The activation of the PPP in HCC is achieved by modulation of several enzymes of the pathway [38], primarily G6PD [39] and transketolase [40]. Isolated hepatocytes utilize about fifteen per cent of glucose in the PPP [41]. In contrast, an increase in PPP activity can be appreciated in the liver of fed mice and hepatoma with respect to non-tumoral counterparts [42]. This suggests that an increase in glucose uptake, typical of a fed state and cancer cells, is necessary to boost the PPP pathway. In addition, cancer cells exploit alternative strategies to re-distribute metabolites towards anabolic pathways diverging from glycolysis. The PKM2 enzyme is highly upregulated in cancer cells because its activity is subjected to complex regulation to modulate glycolytic flux in response to needs [43]. In particular, the inhibitory phosphorylation of PKM2-Tyr105, which we observed to increase in NAT8L-silenced cells, promotes the shuttling of glycolytic metabolites into the PPP [44,45]. The same occurs after phosphorylation of PKM2 serine residues by CDK6 [46] or following cysteine oxidation due to a burst of oxidative stress [47].

Our analysis of NAT8L, ADSL and G6PD protein expression in human HCC biopsies and hepatic nodules of a mouse model of hepatocarcinogenesis further supports the inverse relationship between NAA metabolism and purine biosynthesis in HCC. Reduced levels of NAA were described in pancreatic cancer [48], IDH1-mutated gliomas [49], human and a mouse model of glioblastoma [50,51]. On the other hand, NAA synthesis is augmented in non-small lung and ovarian cancer, in which NAT8L downregulation dampens cell growth [17,18]. In line with the evidence that glutaminolysis is fundamental for aspartate biosynthesis in cancer, NAA overproduction in these tumors mainly derives from the glutamine carbon skeleton. Notably, glucose contribution to aspartate synthesis was augmented in ovarian cancer cells following NAT8L downregulation [18], and glucose represents the physiological source of NAA in the brain and adipocytes [20,52]. Thus, we can speculate that NAA exerts pro-tumoral effects when its synthesis is coupled with glutamine utilization. Consistently, in our experimental conditions and pancreatic cancer, where NAA synthesis is not enhanced, increased proliferation and glutamine addiction correlate with low NAA levels. Moreover, we can assume that in the liver, pancreas, and adipose tissue, which are organs responsible for whole-body homeostasis, NAA may function as a gatekeeper of their great metabolic complexity, differently from the ovary or the lungs, which are metabolically limited to their specific function, and may intensify NAA synthesis for subverting their metabolic constraints and promote tumor development or progression.

5. Conclusions

Our study demonstrates that NAT8L downregulation has a pro-proliferative role in HCC. Cytosolic aspartate availability determined by the impairment of NAA synthesis signals the activation of PPP and purine biosynthetic enzymes. These two events are necessary for boosting nucleotide synthesis and cancer growth. A summary of the proposed metabolic rewiring imposed by NAT8L downregulation in liver cells is presented in Fig. 7. NAT8L could represent a novel checkpoint in limiting aspartate trafficking for nucleotides synthesis and PPP upregulation, two fundamental metabolic traits to exploit as therapeutic strategies against HCC.

Funding

This work was supported by the Italian Association for Cancer Research (AIRC, IG 15403) and MIUR/PRIN 2017 (n. 2017A5TXC3).

Ethics approval and consent to participate

The use of clinical samples was approved by the ethics committee of Regina Elena Tumor Institute. The murine experimentation was performed in accordance with the regulations for the care of human animals and after approval by the Italian Ministry of Welfare Committee and the

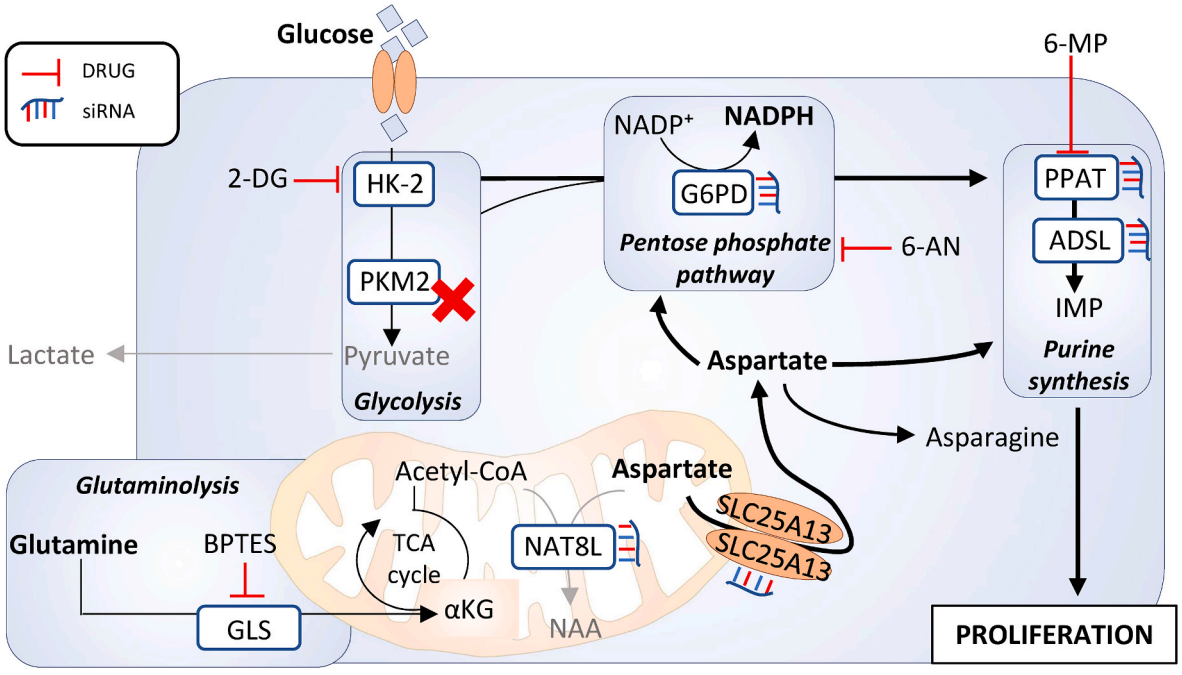

Fig. 7. Schematic representation of the results. Hindering NAA synthesis through NAT8L silencing in HCC favours the efflux of mitochondrial aspartate not used by NAT8L. Once into the cytoplasm, aspartate signals the channelling of glucose into the pentose phosphate pathway boosting, in turn, purine biosynthesis. Mitochondrial metabolism in NAT8L-silenced cells is supported by increased glutaminolysis that can replenish Krebs cycle with α-KG. The inhibition of pathways affected by NAT8L downregulation, via drug inhibitors or siRNAs, can counteract the proliferation rate of NAT8L-silenced cells.

Institutional Animal Care and Use Committee of the University of Rome 'Tor Vergata' (Italy).

Consent for publication

All authors are aware of their work and approve of the content of the article and the fact that they are listed as authors of the article.

Availability of data and materials

All experiments performed and analyzed during this study are included in the currently published article and its additional files. The datasets analyzed in the present study are available in the Cancer Genome Atlas Liver Hepatocellular Carcinoma (TCGA-LIHC) and Gene Expression Omnibus repository (GEO; http://www.ncbi.nlm.nih.gov/geo, accession number GSE82177 and GSE124535).

Authors' contributions

P.D.F. designed and managed the experiments, performed the statistical analysis, conceptualized data and wrote the original draft; S.C. performed and analyzed experiments of enzymatic activity; E.D. performed the bioinformatic analysis; F.F. provided methodological support; G.L. performed HPLC analysis; I.S. performed Seahorse analysis; F. C. and M.R.C. performed study concept and design, edited and reviewed the manuscript; M.R.C. acquired funding. F.C. and M.R.C. equally contributed as co-last authors. All authors read and approved the final manuscript.

Declaration of competing interest

The authors declare that they have no known competing interests to disclose that could influence the work reported in this paper.

Data availability

Data will be made available on request.

Acknowledgements

We thank Prof. Gian Luca Grazi for providing us with the human HCC samples, Prof. Atsumi Nitta for NAT8L/SHATI plasmid, and Dr Vittoria Infantino for the siRNA of SLC25A13.

Pamela De Falco and Federica Felice are enrolled in PhD Program in Cellular and Molecular Biology, Department of Biology, University of Rome "Tor Vergata", Rome, Italy.

Appendix A. Supplementary data

Supplementary data to this article can be found online at https://doi.org/10.1016/j.redox.2022.102585.

References

[1] J.M. Llovet, R.K. Kelley, A. Villanueva, A.G. Singal, E. Pikarsky, S. Roayaie, R. Lencioni, K. Koike, J. Zucman-Rossi, R.S. Finn, Hepatocellular carcinoma, Nat. Rev. Dis. Prim. 7 (2021) 1–28, https://doi.org/10.1038/s41572-020-00240-3.

[2] H. Suzuki, M. Kohjima, M. Tanaka, T. Goya, S. Itoh, T. Yoshizumi, M. Mori, M. Tsuda, M. Takahashi, M. Kurokawa, K. Imoto, S. Tashiro, A. Kuwano, M. Kato, S. Okada, M. Nakamuta, Y. Ogawa, Metabolic alteration in hepatocellular carcinoma: mechanism of lipid accumulation in well-differentiated hepatocellular carcinoma, Chin. J. Gastroenterol. Hepatol. 2021 (2021), 8813410, https://doi.org/10.1155/2021/8813410.

[3] J.D. Yang, P. Hainaut, G.J. Gores, A. Amadou, A. Plymoth, L.R. Roberts, A global view of hepatocellular carcinoma: trends, risk, prevention and management, Nat. Rev. Gastroenterol. Hepatol. 16 (2019) 589–604, https://doi.org/10.1038/s41575-019-0186-y.

[4] K. Lohitesh, R. Chowdhury, S. Mukherjee, Resistance a major hindrance to chemotherapy in hepatocellular carcinoma: an insight, Cancer Cell Int. 18 (2018) 44, https://doi.org/10.1186/s12935-018-0538-7.

[5] M.R. Sullivan, M.G. Vander Heiden, Determinants of nutrient limitation in cancer, Crit. Rev. Biochem. Mol. Biol. 54 (2019) 193–207, https://doi.org/10.1080/10409238.2019.1611733.

[6] M.O. Yuneva, T.W.M. Fan, T.D. Allen, R.M. Higashi, D.V. Ferraris, T. Tsukamoto, J. M. Matés, F.J. Alonso, C. Wang, Y. Seo, X. Chen, J.M. Bishop, The metabolic profile of tumors depends on both the responsible genetic lesion and tissue type, Cell Metabol. 15 (2012) 157–170, https://doi.org/10.1016/j.cmet.2011.12.015.

[7] L. Jin, Y. Zhou, Crucial role of the pentose phosphate pathway in malignant tumors, Oncol. Lett. 17 (2019) 4213–4221, https://doi.org/10.3892/ol.2019.10112.

[8] J.B. Spinelli, M.C. Haigis, The multifaceted contributions of mitochondria to cellular metabolism, Nat. Cell Biol. 20 (2018) 745–754, https://doi.org/10.1038/s41556-018-0124-1.

[9] F. Ciccarone, R. Vegliante, L. Di Leo, M.R. Ciriolo, The TCA cycle as a bridge between oncometabolism and DNA transactions in cancer, Semin. Cancer Biol. 47 (2017) 50–56, https://doi.org/10.1016/j.semcancer.2017.06.008.

[10] L.B. Sullivan, D.Y. Gui, A.M. Hosios, L.N. Bush, E. Freinkman, M.G. Vander Heiden, Supporting aspartate biosynthesis is an essential function of respiration in proliferating cells, Cell 162 (2015) 552–563, https://doi.org/10.1016/j.cell.2015.07.017.

[11] K. Birsoy, T. Wang, W.W. Chen, E. Freinkman, M. Abu-Remaileh, D.M. Sabatini, An essential role of the mitochondrial electron transport chain in cell proliferation is to enable aspartate synthesis, Cell 162 (2015) 540–551, https://doi.org/10.1016/j.cell.2015.07.016.

[12] L. Xu, J. Chen, L. Jia, X. Chen, F. Awaleh Moumin, J. Cai, SLC1A3 promotes gastric cancer progression via the PI3K/AKT signalling pathway, J. Cell Mol. Med. 24 (2020) 14392–14404, https://doi.org/10.1111/jcmm.16060.

[13] T. Bertero, W.M. Oldham, E.M. Grasset, I. Bourget, E. Boulter, S. Pisano, P. Hofman, F. Bellvert, G. Meneguzzi, D.V. Bulavin, S. Estrach, C.C. Feral, S. Y. Chan, A. Bozec, C. Gaggioli, Tumor-stroma mechanics coordinate amino acid availability to sustain tumor growth and malignancy, Cell Metabol. 29 (2019) 124–140, https://doi.org/10.1016/j.cmet.2018.09.012, e10.

[14] M. Tajan, A.K. Hock, J. Blagih, N.A. Robertson, C.F. Labuschagne, F. Kruiswijk, T. J. Humpton, P.D. Adams, K.H. Vousden, A role for p53 in the adaptation to glutamine starvation through the expression of SLC1A3, Cell Metabol. 28 (2018) 721–736, https://doi.org/10.1016/j.cmet.2018.07.005, e6.

[15] J. Garcia-Bermudez, L. Baudrier, K. La, X.G. Zhu, J. Fidelin, V.O. Sviderskiy, T. Papagiannakopoulos, H. Molina, M. Snuderl, C.A. Lewis, R.L. Possemato, K. Birsoy, Aspartate is a limiting metabolite for cancer cell proliferation under hypoxia and in tumours, Nat. Cell Biol. 20 (2018) 775–781, https://doi.org/10.1038/s41556-018-0118-z.

[16] J.R. Moffett, B. Ross, P. Arun, C.N. Madhavarao, M.A.A. Namboodiri, N-acetylaspartate in the CNS: from neurodiagnostics to neurobiology, Prog. Neurobiol. 81 (2007) 89–131, https://doi.org/10.1016/j.pneurobio.2006.12.003.

[17] T.-F. Lou, D. Sethuraman, P. Dospoy, P. Srivastva, H.S. Kim, J. Kim, X. Ma, P.-H. Chen, K.E. Huffman, R.E. Frink, J.E. Larsen, C. Lewis, S.-W. Um, D.-H. Kim, J.-M. Ahn, R.J. DeBerardinis, M.A. White, J.D. Minna, H. Yoo, Cancer-specific production of N-acetylaspartate via NAT8L overexpression in non-small cell lung cancer and its potential as a circulating biomarker, Cancer Prev. Res. 9 (2016) 43–52, https://doi.org/10.1158/1940-6207.CAPR-14-0287.

[18] B. Zand, R.A. Previs, N.M. Zacharias, R. Rupaimoole, T. Mitamura, A.S. Nagaraja, M. Guindani, H.J. Dalton, L. Yang, J. Baddour, A. Achreja, W. Hu, C.V. Pecot, C. Ivan, S.Y. Wu, C.R. McCullough, K.M. Gharpure, E. Shoshan, S. Pradeep, L. S. Mangala, C. Rodriguez-Aguayo, Y. Wang, A.M. Nick, M.A. Davies, G. Armaiz-Pena, J. Liu, S.K. Lutgendorf, K.A. Baggerly, M.B. Eli, G. Lopez-Berestein, D. Nagrath, P.K. Bhattacharya, A.K. Sood, Role of increased n-acetylaspartate levels in cancer, J. Natl. Cancer Inst. 108 (2016) djv426, https://doi.org/10.1093/jnci/djv426.

[19] J.G. Bogner-Strauss, N-acetylaspartate metabolism outside the brain: lipogenesis, histone acetylation, and cancer, Front. Endocrinol. 8 (2017) 240, https://doi.org/10.3389/fendo.2017.00240.

[20] K. Huber, D.C. Hofer, S. Trefely, H.J. Pelzmann, C. Madreiter-Sokolowski, M. Duta-Mare, S. Schlager, G. Trausinger, S. Stryeck, W.F. Graier, D. Kolb, C. Magnes, N. W. Snyder, A. Prokesch, D. Kratky, T. Madl, K.E. Wellen, J.G. Bogner-Strauss, N-acetylaspartate pathway is nutrient responsive and coordinates lipid and energy metabolism in brown adipocytes, Biochim. Biophys. Acta Mol. Cell Res. 1866 (2019) 337–348, https://doi.org/10.1016/j.bbamcr.2018.08.017.

[21] L. Di Leo, R. Vegliante, F. Ciccarone, I. Salvatori, M. Scimeca, E. Bonanno, A. Sagnotta, G.L. Grazi, K. Aquilano, M.R. Ciriolo, Forcing ATGL expression in hepatocarcinoma cells imposes glycolytic rewiring through PPAR-α/p300-mediated acetylation of p53, Oncogene 38 (2019) 1860–1875, https://doi.org/10.1038/s41388-018-0545-0.

[22] OliverH. Lowry, NiraJ. Rosebrough, A.L. Farr, RoseJ. Randall, Protein measurement with the folin phenol reagent, J. Biol. Chem. 193 (1951) 265–275, https://doi.org/10.1016/S0021-9258(19)52451-6.

[23] G. Lazzarino, A.M. Amorini, G. Fazzina, R. Vagnozzi, S. Signoretti, S. Donzelli, E. Di Stasio, B. Giardina, B. Tavazzi, Single-sample preparation for simultaneous cellular redox and energy state determination, Anal. Biochem. 322 (2003) 51–59, https://doi.org/10.1016/j.ab.2003.07.013.

[24] A.M. Amorini, G. Lazzarino, V. Di Pietro, S. Signoretti, G. Lazzarino, A. Belli, B. Tavazzi, Severity of experimental traumatic brain injury modulates changes in concentrations of cerebral free amino acids, J. Cell Mol. Med. 21 (2017) 530–542, https://doi.org/10.1111/jcmm.12998.

[25] B. Tavazzi, G. Lazzarino, P. Leone, A.M. Amorini, F. Bellia, C.G. Janson, V. Di Pietro, L. Ceccarelli, S. Donzelli, J.S. Francis, B. Giardina, Simultaneous high performance liquid chromatographic separation of purines, pyrimidines, N-acetylated amino acids, and dicarboxylic acids for the chemical diagnosis of inborn errors of metabolism, Clin. Biochem. 38 (2005) 997–1008, https://doi.org/10.1016/j.clinbiochem.2005.08.002.

[26] H.F. Alkan, K.E. Walter, A. Luengo, C.T. Madreiter-Sokolowski, S. Stryeck, A. N. Lau, W. Al-Zoughbi, C.A. Lewis, C.J. Thomas, G. Hoefler, W.F. Graier, T. Madl, M.G. Vander Heiden, J.G. Bogner-Strauss, Cytosolic aspartate availability determines cell survival when glutamine is limiting, Cell Metabol. 28 (2018) 706–720, https://doi.org/10.1016/j.cmet.2018.07.021, e6.

[27] V. Infantino, F. Dituri, P. Convertini, A. Santarsiero, F. Palmieri, S. Todisco, S. Mancarella, G. Giannelli, V. Iacobazzi, Epigenetic upregulation and functional role of the mitochondrial aspartate/glutamate carrier isoform 1 in hepatocellular carcinoma, Biochim. Biophys. Acta (BBA) - Mol. Basis Dis. 1865 (2019) 38–47, https://doi.org/10.1016/j.bbadis.2018.10.018.

[28] Y. Natsumeda, N. Prajda, J.P. Donohue, J.L. Glover, G. Weber, Enzymic capacities of purine de Novo and salvage pathways for nucleotide synthesis in normal and neoplastic tissues, Cancer Res. 44 (1984) 2475–2479.

[29] T. Yamaoka, M. Kondo, S. Honda, H. Iwahana, M. Moritani, S. Ii, K. Yoshimoto, M. Itakura, Amidophosphoribosyltransferase limits the rate of cell growth-linked de novo purine biosynthesis in the presence of constant capacity of salvage purine biosynthesis, J. Biol. Chem. 272 (1997) 17719–17725, https://doi.org/10.1074/jbc.272.28.17719.

[30] M. Kondo, T. Yamaoka, S. Honda, Y. Miwa, R. Katashima, M. Moritani, K. Yoshimoto, Y. Hayashi, M. Itakura, The rate of cell growth is regulated by purine biosynthesis via ATP production and G1 to S phase Transition 1, J. Biochem. 128 (2000) 57–64, https://doi.org/10.1093/oxfordjournals.jbchem.a022730.

[31] L.B. Sullivan, A. Luengo, L.V. Danai, L.N. Bush, F.F. Diehl, A.M. Hosios, A.N. Lau, S. Elmiligy, S. Malstrom, C.A. Lewis, M.G. Vander Heiden, Aspartate is an endogenous metabolic limitation for tumour growth, Nat. Cell Biol. 20 (2018) 782–788, https://doi.org/10.1038/s41556-018-0125-0.

[32] P. Borst, The malate-aspartate shuttle (Borst cycle): how it started and developed into a major metabolic pathway, IUBMB Life 72 (2020) 2241–2259, https://doi.org/10.1002/iub.2367.

[33] A.S. Krall, S. Xu, T.G. Graeber, D. Braas, H.R. Christofk, Asparagine promotes cancer cell proliferation through use as an amino acid exchange factor, Nat. Commun. 7 (2016), 11457, https://doi.org/10.1038/ncomms11457.

[34] A.S. Krall, P.J. Mullen, F. Surjono, M. Momcilovic, E.W. Schmid, C.J. Halbrook, A. Thambundit, S.D. Mittelman, C.A. Lyssiotis, D.B. Shackelford, S.R.V. Knott, H. R. Christofk, Asparagine couples mitochondrial respiration to ATF4 activity and tumor growth, Cell Metabol. 33 (2021) 1013–1026, https://doi.org/10.1016/j.cmet.2021.02.001, e6.

[35] Y. Zhou, H. Yu, S. Cheng, Y. Chen, L. He, J. Ren, X. He, J. Chen, L. Zheng, F. Li, Glutamate dehydrogenase 1 mediated glutaminolysis sustains HCC cells survival under glucose deprivation, J. Cancer 13 (2022) 1061–1072, https://doi.org/10.7150/jca.64195.

[36] R.A. Egnatchik, A.K. Leamy, S.A. Sacco, Y.E. Cheah, M. Shiota, J.D. Young, Glutamate-oxaloacetate transaminase activity promotes palmitate lipotoxicity in rat hepatocytes by enhancing anaplerosis and citric acid cycle flux, J. Biol. Chem. 294 (2019) 3081–3090, https://doi.org/10.1074/jbc.RA118.004869.

[37] D. Patel, D. Menon, E. Bernfeld, V. Mroz, S. Kalan, D. Loayza, D.A. Foster, Aspartate rescues S-phase arrest caused by suppression of glutamine utilization in KRas-driven cancer cells, J. Biol. Chem. 291 (2016) 9322–9329, https://doi.org/10.1074/jbc.M115.710145.

[38] M.A. Kowalik, A. Columbano, A. Perra, Emerging role of the pentose phosphate pathway in hepatocellular carcinoma, Front. Oncol. 7 (2017) 87, https://doi.org/10.3389/fonc.2017.00087.

[39] M. Lu, L. Lu, Q. Dong, G. Yu, J. Chen, L. Qin, L. Wang, W. Zhu, H. Jia, Elevated G6PD expression contributes to migration and invasion of hepatocellular carcinoma cells by inducing epithelial-mesenchymal transition, Acta Biochim. Biophys. Sin. 50 (2018) 370–380, https://doi.org/10.1093/abbs/gmy009.

[40] Z. Qin, C. Xiang, F. Zhong, Y. Liu, Q. Dong, K. Li, W. Shi, C. Ding, L. Qin, F. He, Transketolase (TKT) activity and nuclear localization promote hepatocellular carcinoma in a metabolic and a non-metabolic manner, J. Exp. Clin. Cancer Res. 38 (2019) 154, https://doi.org/10.1186/s13046-019-1131-1.

[41] N.Z. Baquer, M. Cascales, B.C. Teo, P. McLean, The activity of the pentose phosphate pathway in isolated liver cells, Biochem. Biophys. Res. Commun. 52 (1973) 263–269, https://doi.org/10.1016/0006–291x(73)90982-0.

[42] M.H. Lee, C.R. Malloy, I.R. Corbin, J. Li, E.S. Jin, Assessing the pentose phosphate pathway using [2, 3-13 C2]glucose, NMR Biomed. 32 (2019), e4096, https://doi.org/10.1002/nbm.4096.

[43] K. Zahra, T. Dey, null Ashish, S.P. Mishra, U. Pandey, Pyruvate kinase M2 and cancer: the role of PKM2 in promoting tumorigenesis, Front. Oncol. 10 (2020) 159, https://doi.org/10.3389/fonc.2020.00159.

[44] T. Hitosugi, S. Kang, M.G. Vander Heiden, T.-W. Chung, S. Elf, K. Lythgoe, S. Dong, S. Lonial, X. Wang, G.Z. Chen, J. Xie, T.-L. Gu, R.D. Polakiewicz, J.L. Roesel, T. J. Boggon, F.R. Khuri, D.G. Gilliland, L.C. Cantley, J. Kaufman, J. Chen, Tyrosine phosphorylation inhibits PKM2 to promote the Warburg effect and tumor growth, Sci. Signal. 2 (2009) ra73, https://doi.org/10.1126/scisignal.2000431.

[45] B. Kumar, R.N.K. Bamezai, Moderate DNA damage promotes metabolic flux into PPP via PKM2 Y-105 phosphorylation: a feature that favours cancer cells, Mol. Biol. Rep. 42 (2015) 1317–1321, https://doi.org/10.1007/s11033-015-3876-8.

[46] H. Wang, B.N. Nicolay, J.M. Chick, X. Gao, Y. Geng, H. Ren, H. Gao, G. Yang, J. A. Williams, J.M. Suski, M.A. Keibler, E. Sicinska, U. Gerdemann, W.N. Haining, T. M. Roberts, K. Polyak, S.P. Gygi, N.J. Dyson, P. Sicinski, The metabolic function of cyclin D3-CDK6 kinase in cancer cell survival, Nature 546 (2017) 426–430, https://doi.org/10.1038/nature22797.

[47] D. Anastasiou, G. Poulogiannis, J.M. Asara, M.B. Boxer, J. Jiang, M. Shen, G. Bellinger, A.T. Sasaki, J.W. Locasale, D.S. Auld, C.J. Thomas, M.G. Vander Heiden, L.C. Cantley, Inhibition of pyruvate kinase M2 by reactive oxygen species contributes to cellular antioxidant responses, Science 334 (2011) 1278–1283, https://doi.org/10.1126/science.1211485.

[48] C.-K. Chang, T.T.-F. Shih, Y.-W. Tien, M.-C. Chang, Y.-T. Chang, S.-H. Yang, M.-F. Cheng, B.-B. Chen, Metabolic alterations in pancreatic cancer detected by in vivo 1H-MR spectroscopy: correlation with normal pancreas, PET metabolic activity, clinical stages, and survival outcome, Diagnostics 11 (2021) 1541, https://doi.org/10.3390/diagnostics11091541.

[49] Z.J. Reitman, G. Jin, E.D. Karoly, I. Spasojevic, J. Yang, K.W. Kinzler, Y. He, D. D. Bigner, B. Vogelstein, H. Yan, Profiling the effects of isocitrate dehydrogenase 1 and 2 mutations on the cellular metabolome, Proc. Natl. Acad. Sci. U. S. A. 108 (2011) 3270–3275, https://doi.org/10.1073/pnas.1019393108.

[50] J.M. Kampa, U. Kellner, C. Marsching, C. Ramallo Guevara, U.J. Knappe, M. Sahin, M. Giampà, K. Niehaus, H. Bednarz, Glioblastoma multiforme: metabolic differences to peritumoral tissue and IDH-mutated gliomas revealed by mass spectrometry imaging, Neuropathology 40 (2020) 546–558, https://doi.org/10.1111/neup.12671.

[51] M. Dilillo, R. Ait-Belkacem, C. Esteve, D. Pellegrini, S. Nicolardi, M. Costa, E. Vannini, E.L. de Graaf, M. Caleo, L.A. McDonnell, Ultra-high mass resolution MALDI imaging mass spectrometry of proteins and metabolites in a mouse model of glioblastoma, Sci. Rep. 7 (2017) 603, https://doi.org/10.1038/s41598-017-00703-w.

[52] A. Moreno, B.D. Ross, S. Blüml, Direct determination of the N-acetyl-L-aspartate synthesis rate in the human brain by (13)C MRS and [1-(13)C]glucose infusion, J. Neurochem. 77 (2001) 347–350, https://doi.org/10.1046/j.1471-4159.2001.t01-1-00282.x.